Dual action of sphinganine in the plant disease resistance to bacteria

Huby Eloïse[1,2], Villaume Sandra[1], Chemotti Catherine[2], Dorey Stéphan[1], Cordelier Sylvain[1], Crouzet Jérôme[1], Gilliard Guillaume[2], Terryn Christine[3], Berquand Alexandre [4], Herrfurth Cornelia[5,6], Feussner Ivo[5,6,7], Jacquard Cédric[1], Fontaine Florence[1], Clément Christophe[1], Baillieul Fabienne[1], Deleu Magali[2*], Dhondt-Cordelier Sandrine[1*]

[1]Université de Reims Champagne-Ardenne, INRAE, RIBP USC 1488, 51100 Reims, France.
[2]Laboratoire de Biophysique Moléculaire aux Interfaces (LBMI), Gembloux Agro-Bio Tech, Université de Liège, 2 Passage des déportés, 5030 Gembloux, Belgium.
[3]Université de Reims Champagne-Ardenne, PICT Platform, 51100 Reims, France.
[4]Université de Reims Champagne-Ardenne, Laboratoire de Recherche en NanoScience EA4682/Nano'Mat, 51100 Reims, France.
[5]University of Goettingen, Albrecht-von-Haller-Institute for Plant Sciences, Department of Plant Biochemistry, Justus-von-Liebig-Weig 11, D-37077, Goettingen, Germany.
[6]University of Goettingen, Goettingen Center for Molecular Biosciences (GZMB), Service Unit for Metabolomics and Lipidomics, Justus-von-Liebig-Weg 11, D-37077, Goettingen, Germany.
[7]University of Goettingen, Goettingen Center for Molecular Biosciences (GZMB), Department of Plant Biochemistry, Justus-von-Liebig-Weg 11, D-37077, Goettingen, Germany.

* MD and SDC contributed equally

* Corresponding authors: Sandrine Dhondt-Cordelier (sandrine.cordelier@univ-reims.fr) and Magali Deleu (Magali.Deleu@uliege.be)

Short Title: Sphingolipids in plant defense responses

ABSTRACT

Sphingolipids are ubiquitous, highly diverse molecules constituting at least 40% of plant plasma membranes. Initially known as modulators of membrane integrity, they now emerge as important players in plant responses to (a)biotic stresses. The interaction between *Arabidopsis thaliana* and the bacterium *Pseudomonas syringae* pv. *tomato* DC3000 *AvrRpm1* (*Pst AvrRpm1*) culminates in the activation of a programmed cell death known as the hypersensitive response, which is part of the plant immune response. In this study, we showed that the co-infiltration of *Pst AvrRpm1*

and sphinganine (d18:0) in *Arabidopsis* leaves suppress the hypersensitive response. This suppression phenotype is also observed with bacteria carrying the effectors AvrB and AvrPphB but not with the ones carrying AvrRpt2 and AvrRps4. Sphingolipid-induced hypersensitive response suppression by *Pst AvrRpm1* is correlated with the down-regulation of the gene *AtNMT1* encoding a *N*-myristoyltransferase. d18:0 does not have a direct antibacterial effect and its co-infiltration in plants does not display typical signs of immune response such as activation of salicylic acid signaling pathway and extracellular reactive oxygen species production. Biophysical studies showed that d18:0 interacts with plant plasma membrane lipids. More specifically, d18:0 disturbs plant plasma membrane organization and mechanical properties. Our results demonstrate that sphingolipids play an important role in plant resistance, especially by interfering with the plasma membrane organization and effector localization and thus disturbing their function and subsequent immune responses.

Keywords: sphingolipids, biophysics, plant immunity, effectors, plasma membrane

54 **INTRODUCTION**

55 Recognition of pathogenic microorganisms leading to plant immunity is commonly
56 divided into two pathways that can mutually potentiate each other (Ngou *et al*., 2021).
57 Pathogen perception involves the recognition of pathogen-associated molecular
58 patterns (PAMPs) through plant cell surface-anchored pattern recognition receptors
59 (PRRs), which induces pattern-triggered immunity (PTI) (Saijo and Loo, 2020).
60 However, some bacteria can interfere with PTI by delivering effectors into the plant cell
61 to block signaling mechanisms at different steps (Desveaux *et al*., 2006; Kamoun,
62 2006; Dodds *et al*., 2009). The recognition of microbial effectors or virulence factors by
63 the plant cells through intracellular nucleotide-binding leucine-rich repeat receptors
64 (NLRs) induces effector-triggered immunity (ETI). PTI and ETI share many signals and
65 components, but their signaling pathways are induced at different scales and time
66 (Bjornson and Zipfel, 2021; Kadota *et al*., 2019; Yuan *et al*., 2021). Typical overlaps in
67 signaling components are e.g., the production of reactive oxygen species (ROS), the
68 influx of calcium, or mitogen-activated protein kinase (MAPK) signaling cascades. They
69 also share some immune responses, such as transcriptional reprogramming and
70 alterations in stress-related hormone homeostasis, including salicylic acid (SA),
71 jasmonic acid (JA), and/or ethylene (ET) (Bari and Jones, 2009; Betsuyaku *et al*., 2018;
72 Guan *et al*., 2015). Rapid programmed cell death (PCD) at the site of infection, known
73 as the hypersensitive response (HR), usually is a hallmark of the ETI pathway (Couto
74 and Zipfel, 2016; Henry *et al*., 2013; Kadota *et al*., 2019; Ngou *et al*., 2021; Yuan *et al*.,
75 2021).

76 The bacterial pathogen *Pseudomonas syringae* pv. *tomato* DC3000 (*Pst* DC3000) has
77 been extensively studied due to its capacity to cause bacterial speck in both tomato
78 and *Arabidopsis thaliana* (hereafter *Arabidopsis*) (Lee *et al*., 2015; Wei *et al*., 2018),

79 as well as the availability of its complete genome sequence (Buell *et al*., 2003).
80 Transformation of *Pst* DC3000 to express effectors has been essential for the
81 discovery of mechanisms associated with ETI (Boyle and Martin, 2015; Hicks and
82 Galán, 2013; Nimchuk *et al*., 2000). AvrRpm1 effector was originally identified in *P.*
83 *syringae* pv. *maculicola* strain m2 (Debener *et al*., 1991) and harbors an N-terminal
84 eukaryotic consensus site for myristoylation required for its full avirulence function. This
85 allows the effector, once acylated by the plant host, to be redirected to the plant plasma
86 membrane (PM) (Boyle and Martin, 2015; Hicks and Galán, 2013; Nimchuk *et al*.,
87 2000). Although the host acylation apparatus is initially exploited by bacteria to interfere
88 with PTI by binding to the kinase domain of PRRs (Boyle and Martin, 2015), in resistant
89 plants, it can actually turn against the pathogen. For instance, the NLR RPM1
90 (RESISTANCE TO *PSEUDOMONAS SYRINGAE* PV *MACULICOLA*) in *Arabidopsis*,
91 is monitored by the PM-associated protein RPM1-INTERACTING PROTEIN-4 (RIN4),
92 which guards it against effector-mediated perturbations (Boyes *et al*., 1998; Jones and
93 Dangl, 2006; Mackey *et al*., 2002). Therefore, once relocated to the PM, AvrRpm1 will
94 target RIN4, inducing its phosphorylation. This activates RPM1 which triggers the ETI
95 and the HR, together interrupting the bacterial spread of the and leading to the
96 degradation of RPM1 (Boyes *et al*., 1998; Mackey *et al*., 2002; Xin *et al*., 2018).
97 Sphinganine is a sphingolipid (SL), belonging to the long-chain base (LCB) class,
98 which are one major building block of SLs (Pata *et al*., 2010). It consists of a C18 core
99 with an amino group at C2 and two hydroxylations at C2 and C3 (Luttgeharm *et al*.,
100 2016; Mamode Cassim *et al*., 2019). SLs are key components of the plant PM
101 structure, accounting for up to 40 mol% of its external leaflet (Cacas *et al*., 2016). They
102 are found mostly in lipid microdomains, and play an important part in signaling, protein
103 aggregation, and stress response (Cacas *et al*., 2016; Grennan, 2007; Mamode

104 Cassim *et al*., 2019; Pata *et al*., 2010). Recent studies have shown that SLs are key
105 players in PCD regulation occurring either during plant development or immunity (Ali
106 *et al*., 2018; Berkey *et al*., 2012; Huby *et al*., 2020; Lenarčič *et al*., 2017). For instance,
107 Bax-inhibitor-1 interacts with enzymes of the SL biosynthetic pathway FAH1 and 2
108 (FATTY ACID HYDROXYLASE 1 and 2). It leads to changes in lipid content of
109 membrane microdomains (Lenarčič *et al*., 2017). This causes the loss of proteins
110 normally located in these microdomains and which are essential for plant defense,
111 especially for cell death by oxidative stress or SA (Ishikawa *et al*., 2015). Further links
112 between PCD, sphingolipids and the SA pathway have recently been highlighted. In
113 *Arabidopsis*, triple mutations of enzymes of the SL biosynthetic pathway, FAH1, FAH2
114 and LOH2 (LAG ONE HOMOLOG 2) led to the accumulation of sphinganine and
115 ceramides, another class of SLs. These mutants also exhibited a PCD that was
116 dependent on SA and was probably linked to d18:0 accumulation (König *et al*., 2021,
117 2012).
118 Sensing of pathogen-derived lipid molecules is far from being elucidated. A recent
119 study demonstrated that the clivage product of the *Phytophthora infestans* ceramide D
120 by the neutral ceramidase 2 is recognized by the PRR RESISTANT TO DFPM-
121 INHIBITION OF ABSCISSIC ACID SIGNALING 2 (RDA2) (Kato *et al*., 2022). Some
122 studies suggest that lipidic elicitors can directly interact with lipids in the plant PMs
123 (Cordelier *et al*., 2022). For instance, ergosterol, the main sterol of fungi, is described
124 as a general elicitor of plant defenses (Klemptner *et al*., 2014). Due to its lipidic nature
125 and its capacity to form rafts, it is thought to interact with the PM. In *Beta vulgaris,* it
126 can inhibit its H^+-ATPase activity, supposedly by tempering with the NADPH oxidase
127 present in the plant microdomains (Hao *et al*., 2014; Rossard *et al*., 2010).

128 While there are abundant reports on the links between LCBs and PCD (Ali *et al*., 2018;
129 Huby *et al*, 2020), only few data on the use of exogenously applied LCBs and their
130 mode of action are available (Glenz *et al*., 2019; Gutiérrez-Nájera *et al*., 2020; Magnin-
131 Robert *et al*., 2015; Peer *et al*., 2011; Saucedo-García *et al*., 2011, 2023; Shi *et al*.,
132 2007). In previous studies, we and others have shown that the co-infiltration of
133 *Arabidopsis* leaves with an LCB and *Pst AvrRpm1* does not induce an HR (Glenz *et*
134 *al*., 2022; Magnin-Robert *et al*., 2015). In order to decipher the underlying mechanism,
135 the activation of canonical defense responses and antibacterial effect of the LCB were
136 analyzed. Moreover, we showed similar phenotype with other effectors that share the
137 myristoylation sequence with AvrRpm1. Finally, biophysical analyses demonstrated
138 that sphinganine can interact with the plant biomimetic PM and disturb its organization
139 as well as its mechanical features.
140

141 **RESULTS**

142 **Effect of *Pst AvrRpm1* and sphinganine co-infiltration on *Arabidopsis* cell death**

143 We and others previously demonstrated that the co-infiltration of *Pst AvrRpm1* and
144 d18:0 or t18:0, respectively, does not induce an HR in contrast to what happens with
145 an infiltration of an avirulent bacteria or LCB alone (Magnin-Robert *et al.*, 2015; Glenz
146 *et al*., 2022). Therefore, *Pst* expressing effectors other than AvrRpm1 were selected to
147 elucidate whether the absence of visible HR was dependent on the effector. AvrRpt2
148 was chosen because, like AvrRpm1, it is associated to the PM with RIN4 (Boyes *et al*.,
149 1998; Mackey *et al*., 2003; Xin *et al*., 2018). AvrRps4 was also tested because of the
150 cytoplasmic localization of its target, RPS4 (Gassmann *et al*., 1999; Wirthmueller *et al*.,
151 2007).

152 As expected, treatment with *Pst* DC3000 co-infiltrated or not with d18:0 triggered
153 typical disease symptoms and infection with *Pst AvrRpm1*, *Pst AvrRpt2* or *Pst AvrRps4*
154 alone, gave rise to a typical HR. Whereas co-infiltration of *Pst AvrRpm1* and d18:0 did
155 not induce a visible HR as expected, the other tested bacteria displayed an HR when
156 co-infiltrated with the sphingolipid (Fig. 1A). Changes in conductivity were then used
157 as a marker of plant cell death, as PM damages result in strong electrolyte leakage
158 (Kawasaki *et al*., 2005) (Fig. 1B). All treatments triggered an increase in conductivity
159 between 4 and 24 hpi, except for co-infiltration with *Pst AvrRpm1* and d18:0, displaying
160 a conductivity stable over time and similar to the control plants (Fig. 1B). These findings
161 are consistent with our previous study (Magnin-Robert *et al*., 2015) and corroborated
162 with phenotypic observations in Fig. 1A.

163

164 ***In vitro* and *in planta* growth of *Pst AvrRpm1* in presence of sphinganine**

165 As a potential deleterious effect of d18:0 on the bacteria could not be excluded, *in vitro*
166 bacterial growth measurements were undertaken with or without the sphingolipid in the
167 culture medium (Fig. 2A). Ethanol had no effect on bacterial growth of all tested strains
168 (data not shown). Interestingly, d18:0 had no antibacterial effect on *Pst AvrRpm1* and
169 out of all the bacteria tested, d18:0 slightly reduced the growth rate of *Pst AvrRpt2*.
170 Surprisingly, this bacterium does provoke cell death when co-infiltrated into leaves.
171 To determine the effect of the co-infiltration on bacterial growth *in planta*, bacterial
172 populations were quantified at 0 and 48 hpi (Fig. 2B). The growth of the avirulent strain
173 *Pst AvrRpm1* was slightly reduced compared to the virulent strain, *Pst* DC3000 at 48
174 hpi. Furthermore, while the co-infiltration had no consequence on the development of
175 *Pst* DC3000, it slightly reduced *Pst AvrRpm1* growth at 48 hpi. This bacterial count was
176 however two-fold higher at 48 hpi than at 0 hpi, like in the other conditions (Fig. 2B).
177 Collectively, these data suggest that d18:0 does not have an antibacterial effect that
178 could explain the absence of HR when *Pst AvrRpm1* is co-infiltrated with d18:0.
179 Moreover, while *Pst AvrRpm1* continues its development inside the plant, it is however
180 incapable of triggering an HR.
181

182 **Extracellular ROS production by *Arabidopsis* in response to infection by *Pst***

183 Strong and sustained extracellular ROS production is an early defense event generally
184 linked to HR. We therefore monitored their production by *Arabidopsis* in response to
185 *Pst AvrRpm1*, *Pst AvrRpt2* and *Pst AvrRps4* (Fig. 3). No significant difference was
186 found between ROS production triggered by bacteria alone or mixed with ethanol (data
187 not shown). As already observed by Magnin-Robert *et al.* (2015), co-treatment of *Pst*
188 *AvrRpm1* but also of *Pst AvrRpt2* and *Pst AvrRps4* with d18:0 reduced extracellular
189 ROS production by approximatively 6-, 2- and 1.7-fold, respectively (Fig. 3). Only the

190 co-infiltration of *Pst AvrRpm1* and d18:0 did not result in an HR (Fig. 1) but ROS levels
191 appear to be dramatically affected even with other bacteria like *Pst AvrRps4*. These
192 results suggest that reduced ROS production is not directly linked to the absence of
193 HR.
194
195 **Effects of *Pst AvrRpm1* and sphinganine co-infiltration on *Arabidopsis* late**
196 **defense responses**
197 Considering the effects of d18:0 on ROS production and cell death development, other
198 markers of plant defense were studied in response to co-infiltration. The accumulation
199 of the phytoalexin camalexin as well as the hormones SA and JA-Ile was followed. The
200 expression of *PATHOGENESIS-RELATED GENE 1* (*PR1*) and *VEGETATIVE*
201 *STORAGE PROTEIN 1* (*VSP1*), marker genes of SA and JA-Ile signaling pathways,
202 respectively, was also analyzed. Control infiltration did not induce camalexin
203 production (Fig. 4A). At 48 hpi, *Pst* DC3000 inoculation with or without d18:0 triggered
204 similar camalexin accumulation. However, d18:0 co-infiltration significantly reduced
205 camalexin production in response to *Pst AvrRpm1* since it decreased from ~250 nmol/g
206 FW to a similar level observed in controls (~3 nmol/g FW) at 48 hpi (Fig. 4A).
207 Overexpression of *PR1* was observed 48h after infiltration with each *Pst* strain alone
208 (Fig. 4C), which correlated with the accumulation of SA (Fig. 4E). Neither SA
209 accumulation nor *PR1* expression was induced at earlier time points. The use of an
210 *Arabidopsis* reporter line *PR1::GUS* confirmed the induction of *PR1* expression in
211 treated leaves (Fig. 4B). Both SA accumulation and *PR1* overexpression are repressed
212 when leaves are co-infiltrated with d18:0, leading to similar levels as in control plants
213 (Fig. 4, C and E). *VSP1* is weakly expressed in response to *Pst* DC3000 but
214 overexpressed when this bacterium is co-infiltrated with d18:0 (~ 9-fold and ~ 6-fold

215 more at 6 and 48 hpi, respectively) (Fig. 4D). JA-Ile levels are however higher with the
216 bacterium alone than co-infiltrated (Fig. 4F). When *Arabidopsis* was inoculated with
217 *Pst AvrRpm1*, *VSP1* was slightly overexpressed at 48 hpi but repressed when co-
218 infiltrated with d18:0 (Fig. 4D). JA-Ile levels were concomitantly low (Fig. 4F), as
219 expected from plants challenged with avirulent *P. syringae* (Mur *et al.*, 2006). Overall,
220 co-infiltration of *Pst AvrRpm1* with d18:0 significantly lowers the amount of camalexin
221 and both defense hormone signaling pathways.
222
223 **Involvement of RPM1 and RIN4 in the absence of HR**
224 Once injected into the cytoplasm of the host, AvrRpm1 triggers the phosphorylation of
225 RIN4, inducing the activation of RPM1 and subsequently the ETI leading to an HR
226 (Nimchuck *et al*., 2000). To elucidate whether RPM1 and / or RIN4 were involved when
227 the bacterium is co-infiltrated with d18:0, inoculations of *Pst AvrRpm1* were performed
228 on *Arabidopsis* mutants *rpm1-3,* and *rpm1-rps2-rin4,* as well as the complemented line
229 *RPM1-myc rpm1*. Infiltration of the bacteria alone induced cell death and co-infiltration
230 of the complemented line displayed no symptoms, as expected (Fig. 5A). Despite
231 lacking RPM1 and / or RIN4, all mutants showed the same phenotype as the WT when
232 co-infiltrated with d18:0 as they did not exhibit visible cell death (Fig. 5A). It has been
233 previously demonstrated that RPM1 is degraded during the first hpi, coincidently with
234 the onset of the HR (Boyes *et al*., 1998). To further elucidate the role of RPM1 and
235 RIN4, *RPM1-myc rpm1* plant was used to monitor the degradation of RPM1 following
236 inoculation (Fig. 5B). Western blot analysis showed that while RPM1 was degraded
237 from 4 to 6 hpi when *Pst AvrRpm1* was infiltrated alone, the protein was still detected
238 24 hpi when the bacteria was co-infiltrated (Fig. 5B). Altogether, these data suggest

239 that the mechanism underlying the absence of HR occurs upstream of RPM1
240 degradation.
241
242 **Effect of *Pst AvrB* and *Pst AvrPphB* co-infiltration with sphinganine on**
243 ***Arabidopsis* defense response**
244 The three effectors AvrRpm1, AvrB and AvrPphB share an eukaryotic *N*-myristoylation
245 site in their protein sequences that allows them to be redirected to the PM once they
246 have entered their host (Nimchuk *et al*., 2000). Like AvrRpm1, AvrB interacts with
247 RPM1 and RIN4 (Grant *et al*., 1995; Lee *et al*., 2004), and AvrPphB with RPS5 and
248 PBS1, both located at the PM (Ade *et al*., 2007; Pottinger and Innes, 2020). As already
249 demonstrated (Warren *et al*., 1998; Whalen *et al*., 1991), infiltration of *Pst AvrB* or *Pst*
250 *AvrPphB* triggers an HR. No cell death was visible when both *Pst AvrB* and *Pst*
251 *AvrPphB* were co-infiltrated with d18:0, suggesting HR was not triggered in treated
252 plants, similarly to *Pst AvrRpm1* (Fig. 6A). Further tests were conducted to determine
253 if d18:0 had an *in vitro* effect on these bacteria. Their growth rate remained unchanged
254 after d18:0 addition (Fig. 6B), confirming that d18:0 has no antibacterial effect on these
255 two bacteria. Extracellular ROS production by *Arabidopsis* in response to *Pst AvrB* and
256 *Pst AvrPphB* was also monitored (Fig. 6C). As for *Pst AvrRpm1*, d18:0 significantly
257 reduced this production in response to both bacteria (~ 2-fold for *Pst AvrB* and ~ 3-fold
258 for *Pst AvrPphB*).
259
260 ***NMT1* relative expression following *Pst AvrRpm1* and sphinganine co-infiltration**
261 In *Arabidopsis*, two enzymes, NMT1 and NMT2, are responsible for *N*-myristoylation
262 (Pierre *et al*., 2007). As the corresponding mutants displaying severe phenotypes, they
263 were thus not suitable for our experiments. We used qRT-PCR to determine

264 expression patterns of *NMT1* and *NMT2* in response to infiltration of *Arabidopsis* WT
265 leaves with *Pst* DC3000 or *Pst AvrRpm1*, either alone or with d18:0 (Fig. 7).
266 Unfortunately, the expression of *NMT2* was too low to be detectable. At 6 hpi, *NMT1*
267 expression in plants infiltrated with *Pst* DC3000 alone or with d18:0 was similar to that
268 of control samples but was induced at 48 hpi (~ 2-fold). When plants were infiltrated
269 with *Pst AvrRpm1* alone, a stimulation of *NMT1* expression is observed during the time-
270 course experiment to reach a ~2.2-fold induction at 48 hpi (Fig. 7). However, when
271 plants were co-infiltrated with *Pst AvrRpm1* and d18:0, no induction could be observed
272 during the time-course experiment (Fig. 7). Thus, a decrease of ~1.7-fold is observed
273 48 hpi between *Pst AvrRpm1* infiltrated alone and with d18:0. Overall, these results
274 suggest that co-infiltration with d18:0 modifies *NMT1* expression in response to
275 infection with *Pst AvrRpm1*.
276

277 **Interaction capacity of sphinganine with plant plasma membrane-mimicking**
278 **models**

279 It has been shown that LCB sphingosine (d18:1) can increase the permeability of
280 liposomal and erythrocyte ghost membranes to aqueous solutes (Contreras *et al*.,
281 2006). Based on this finding, d18:0 was hypothesized to interact with the lipids of plant
282 PM. To investigate this hypothesis, we conducted *in silico* and *in vitro* biophysical
283 analyses using membrane plant models. Thanks to their defined structure and
284 controlled lipid composition, these models were found to be useful in understanding
285 how external molecules affect the organization and mechanical properties of the
286 membranes (Deleu *et al*., 2014; Furlan *et al*., 2020; Cordelier *et al*., 2022).

287 The Impala modeling method was used to predict the ability of d18:0 to insert into an
288 implicit model lipid bilayer and to determine the preferable location and positioning of

289 d18:0 within a membrane bilayer (Fig. 8). The more negative the energy is, the more
290 favorable the insertion will be. A sharp drop of energy was observed as d18:0 moved
291 from the aqueous phase to the membrane surface (up to ~-10 Kcal/mol), indicating that
292 it could easily insert into membranes. The energy was close to 0 Kcal/mol in the
293 hydrophobic region of the membrane, suggesting that d18:0 has a less favorable
294 interaction with this region compared with the lipid bilayer hydrophilic region (Fig. 8A).
295 Nevertheless, the non-positive energy value in the hydrophobic region of the bilayer
296 suggests that d18:0 could flip-flop between the two bilayer leaflets. A large increase in
297 energy (from ~-10 Kcal/mol to +6.7 Kcal/mol) is also observed when d18:0 moves from
298 the inner bilayer leaflet to the aqueous medium, which strongly suggests that d18:0
299 has no propensity to cross the membrane and enter into the cytoplasm. The preferred
300 positioning of d18:0 within the membrane is shown in Fig. 8B. Its lipid chain lies within
301 the hydrophobic part of the membrane while the amine and alcohol groups are located
302 in the hydrophilic part of the bilayer. Altogether, this indicates that d18:0 can interact
303 with membranes and remains there. To support these simulation results, experimental
304 analyses were performed using large unilamellar vesicles (LUVs) that mimic plant PM,
305 consisting of palmitoyl-2-linoleoyl-*sn*-glycero-3-phosphocholine (PLPC),
306 glucosylceramide (GluCer) and β-sitosterol (sito) as the plant PM model phospholipid,
307 sphingolipid and sterol respectively (Deleu *et al*., 2014; Rondelli *et al*., 2021; Deboever
308 *et al*., 2022).

309 Results from ITC experiments showed a negative and decreasing heat flow after each
310 LUV injection into the d18:0 solution (Fig. 9A), indicating that d18:0 interacts with plant
311 PM-mimicking LUVs. The thermodynamic parameters calculated from the fitting of raw
312 data are presented in Fig. 9B. The binding coefficient K was relatively high (>80 mM^{-1})
313 suggesting that d18:0 has a strong affinity for plant-mimicking lipid membranes

314 confirming the low probability that it emerges in the intracellular medium. This affinity
315 for plant PM-like liposomes is higher than that observed for other plant-eliciting
316 molecules such as linoleic and linolenic acid hydroperoxides (<3 mM^{-1}; Deleu *et al*.,
317 2019), and rhamnolipid bolaforms (7.5 mM^{-1}; Luzuriaga-Loaiza *et al*., 2018). The
318 binding reaction of d18:0 to LUVs was spontaneous as the molar free energy ΔG was
319 negative, exothermic as the molar enthalpy change ΔH was negative and generated a
320 positive change of the molar entropy (TΔS>0). The higher absolute value of the molar
321 entropy (TΔS>0) compared to the absolute value of the molar enthalpy change (ΔH),
322 indicates that the interactions is entropy-driven, i.e. mostly of hydrophobic nature.
323 Altogether, these results suggest that d18:0 is attracted by and can interact with plant
324 lipid membranes.
325

326 **Lipid specificity of the interaction between sphinganine and plant plasma**
327 **membrane-mimicking models**

328 To investigate specific interactions between d18:0 and lipids representative of plant
329 PM, the Langmuir trough technique was used to analyze the adsorption capacity of
330 d18:0 into monolayers of each individual lipid. In this technique, a lipid monolayer is
331 initially formed at an air-water interface, and then d18:0 is injected into the subphase
332 beneath the monolayer. The increase in surface pressure (ΔΠ) at a constant trough
333 area was monitored to determine the adsorption of d18:0 into the lipid monolayer at
334 different initial surface pressures (Π_i) (Supplemental Fig. S1). Two parameters were
335 determined from these data (Fig. 10A): (i) the differential surface pressure ($d\Pi_0$), which
336 provides information on the attractive effect of the lipids on d18:0, and (ii) the maximal
337 insertion pressure (MIP), which reflects the ability of d18:0 to penetrate into the lipid
338 monolayer (Deleu *et al*., 2014). Upon insertion of d18:0 onto monolayers formed with

339 individual plant PM lipids, $d\Pi_0$ values were all positive and similar for all compositions,
340 indicating that all tested lipids exert a similar attraction on d18:0 (Fig. 10A). MIP values
341 were all higher than the lateral pressure supposed to prevail into biological membranes
342 (30 – 35 mN/m) (Marsh, 1996), meaning that d18:0 may be able to adsorb into natural
343 plant membranes.

344 Lipid specificity of the interaction was also studied by an *in silico* approach using the
345 Hypermatrix docking method. This method calculates the energy of interaction
346 between d18:0 and individual plant lipids at a hydrophilic/hydrophobic interface,
347 indicating whether this interaction is energetically favorable or not (Brasseur *et al*.,
348 1987; Deleu *et al*., 2014). Results showed that the interaction between d18:0 and all
349 plant lipids was favorable as all interaction energies are negative (Fig. 10B).
350 Interestingly, the interaction energies between d18:0 and plant lipids were more
351 favorable than those observed for d18:0 with itself. With this method, interaction
352 between d18:0 and PLPC or GluCer appeared to be more favorable than with β-
353 sitosterol.

354 Altogether, these data showed that d18:0 is attracted by and could interact with lipids
355 of plants. There is however no clear trend to determine a preferential interaction of
356 d18:0 with a particular lipid.

357

358 **Modification of the organization and mechanical properties of plant plasma**
359 **membrane-mimicking models induced by sphinganine**

360 Since d18:0 can interact with lipids found in plant PMs, additional experiments were
361 conducted to investigate how these interactions could impact the mechanical
362 properties and the organization of plant PMs.

363 Two aspects of membrane mechanics were considered: membrane fluidity and
364 membrane elasticity. Membrane fluidity refers to the degree of lipid packing and the
365 mobility or dynamics of lipids within the membrane, which can be characterized by the
366 order level parameter (Gerbeau-Pissot *et al*., 2014). Membrane elasticity
367 corresponding to the resistance of a material to deformation when subjected to an
368 applied force was determined by measuring the Young's modulus. The higher the
369 Young's modulus, the stiffer and less deformable the object is (Magazzu and
370 Marcuello, 2023). Although membrane fluidity can be influenced by the membrane
371 elasticity, there is no direct quantitative relationship between Young's modulus and
372 membrane fluidity or order level and therefore must be considered as separate aspects
373 of membrane behavior.
374 To analyze the order level of *Arabidopsis* PM in response to d18:0, *Arabidopsis* leaf
375 protoplasts were stained with the dye di-4-ANEPPDHQ. The order level of the
376 membrane, revealed by fluorescence imaging, was quantified using the red/green ratio
377 of the membrane (RGM) (Dinic *et al*., 2011; Gerbeau-Pissot *et al*., 2014). Observations
378 of protoplasts indicated a significant decrease in RGM compared to controls (from 0.99
379 to 0.80 and 0.74 for concentrations of 2 µM and 5 µM d18:0, respectively) (Fig. 11A-
380 D), with no statistical difference between the two concentrations of d18:0. The RGM
381 profile of a 4 µm fragment of PM from controls appeared homogenous whereas those
382 from sphingolipid-treated protoplasts is more heterogenous (Fig. 11E-G). These
383 findings suggest that the order level increased in response to the LCB. This increase
384 in membrane order level in the presence of d18:0 was confirmed by the greater
385 variation in the generalized polarization of Laurdan on biomimetic liposomes compared
386 to the control ethanol, and this as soon as d18:0 came into contact with the lipid bilayer
387 (Fig. 11H). Laurdan is a fluorescent probe sensitive to membrane lateral packing, a

388 higher generalized polarization corresponding to a greater lipid packing (Parasassi *et*
389 *al*., 1991).

390 Young's modulus was measured by recording force-distance curves using AFM on leaf
391 protoplasts. In the presence of d18:0, Young's modulus decreased (Fig. 11I) indicating
392 a reduction in membrane elasticity and a lower resistance to membrane deformation.
393 Again, there is no concentration dependence.

394 Using the Big Monolayer simulation method, which is useful for studying the lateral
395 distribution of molecules based on their mutual interaction energies, we observed that
396 d18:0 preferentially interacted with the lipid domains initially formed by β-sitosterol and
397 GluCer (Fig. 11J left), resulting in their fragmentation as shown in Fig. 11J right.
398 Accordingly, fluorescence images of di-4-ANEPPDHQ-stained protoplasts (Fig. 11 A
399 to C and E to G) demonstrated an increase in the number of small ordered domains in
400 the presence of d18:0 compared to its absence.
401
402

403 **DISCUSSION**

404 The roles of sphingolipids during PCD in response to biotic stress are still not fully
405 understood (Berkey *et al*., 2012; Huby *et al*., 2020). Previous studies showed that co-
406 infiltration of *Pst AvrRpm1* with the LCB d18:0 or t18:0 on *Arabidopsis* leaves did not
407 trigger an HR on the treated leaves, with no evidence of cell death, indicating the
408 conservation of plant PM integrity and absence of cell lysis following the co-infiltration
409 (Glenz *et al*., 2022; Magnin-Robert *et al*., 2015). In the present work, we show that the
410 levels of all plant immunity markers in response to co-infiltration, including those related
411 to the plasma membrane, are similar to the control plants, despite the fact that the
412 bacterium still develops inside plant tissues. We also report a similar effect with *Pst*
413 expressing the effector AvrB or AvrPphB. AvrRpm1, AvrB and AvrPphB need to be
414 myristoylated to be active. This process is disturbed during co-infiltration leading to an
415 absence of plant defense response activation. Finally, interaction of d18:0 with lipids
416 of the plant PM was demonstrated.

417 *In vitro* tests showed that this LCB does not have an antibacterial effect on *Pst*
418 *AvrRpm1*, *Pst AvrB* and *Pst AvrPphB*, similarly to results obtained with *P. aeruginosa*
419 (Fischer *et al*., 2012). t18:0 has been shown to inhibit *Pst* growth (Glenz *et al*., 2022).
420 However, the authors used a smaller bacterial concentration and LB medium to
421 perform their tests. Here, by using a higher bacterial concentration and a medium more
422 favorable to *Pst* growth, the bacterial pressure was more important in our tests, which
423 could explain the discrepancy with the data published by Glenz and colleagues (2022).

424 *In planta* experiments showed that, even though *Pst AvrRpm1* is not capable of
425 inducing an HR when co-infiltrated with d18:0, it is still present inside the plant and
426 even continues to thrive, confirming the non-detrimental effect of d18:0 on the
427 bacterium. In contrast, a pre-treatment with FB1, in order to promote endogenous LCB

428 accumulation, inhibit *Pst* DC3000 but not *Pst AvrRpm1* growth (Saucedo-García *et al*.,
429 2023). Moreover, *loh1* plants that accumulate endogenous levels of LCBs together with
430 *PR1* enhanced expression, displays spontaneous cell death (Ternes *et al*., 2011). The
431 localization (apoplastic *vs* cytoplasmic) of the LCB and the fact that FB1 or *loh1* induces
432 or displays higher LCB but also LCB-P, ceramide or GluCer accumulation (Chen *et al*.,
433 2008; Kimberlin *et al*., 2016; Saucedo-García *et al*., 2011) could explain this
434 discrepancy. This could also suggest that interaction of d18:0 with the PM and its
435 presence within the PM when infiltrated could be essential in the cell death induction.
436 Previous results showed that co-treatment of d18:0 with *Pst* DC3000 or with *Pst*
437 *AvrRpm1* drastically reduced extracellular ROS production by *Arabidopsis* (Magnin-
438 Robert *et al*., 2015). Our results demonstrate that d18:0 reduces ROS production in
439 response to bacteria that induce symptoms *in planta* but also to bacteria that do not
440 induce symptoms (*Pst AvrRps4* and *Pst AvrRpm1, Pst AvrB, Pst AvrPphB,*
441 respectively). This production remained unchanged when plants are treated with *Pst*
442 *AvrRpt2*. The hypothesis that LCBs could impact ROS production by plants has already
443 been put forward in several studies, although some of them are somewhat
444 contradictory. Coursol *et al*. (2015) showed that exogenous addition of 20 µM LCBs
445 reduced tobacco ROS production in response to cryptogein. In *Arabidopsis*, LCBs can
446 induce both intracellular as well as extracellular ROS production (Glenz *et al*., 2019;
447 Peer *et al*., 2011; Shi *et al*., 2007; Saucedo-Garcia *et al*., 2023). ROS production can
448 be detected during both PTI and ETI (Torres, 2010). In *Arabidopsis,* it is mainly related
449 to RbohD located in lipid microdomains of the plant PM (Hao *et al*., 2014; Mongrand *et*
450 *al*., 2004). Several studies have suggested that RbohD-derived ROS production is not
451 directly involved in plant cell death, but rather in the signaling pathways associated
452 with plant defense responses (Lherminier *et al*., 2009; Torres *et al*., 2005). This means

453 that even though d18:0 could alter ROS production, it may not have any impact on
454 PCD and would therefore not be responsible for the absence of HR. Additionally, it has
455 been already demonstrated that a lipidic elicitor is able to interact with lipid membrane
456 microdomains (Rossard *et al*., 2010). These data suggest that LCBs might interact with
457 and thus disturb the PM organization of *Arabidopsis* leading to the reduction of RbohD
458 activity.
459 SA pathway is triggered in response to hemibiotrophic pathogens, such as *Pst*,
460 whereas JA and its active form JA-Ile are involved in infection by necrotrophic
461 pathogens (Li *et al*., 2019). In our study, *PR1* is significantly down-regulated upon co-
462 infiltration with d18:0 and *Pst* DC3000, and even more so upon *Pst AvrRpm1,* which
463 coincides with lower SA accumulation. SA repression is commonly associated with
464 promotion of bacterial development and/or enhancement of a JA-dependent pathway
465 (Brooks *et al*., 2005; Moore *et al*., 1989; Zhou *et al*., 1998). *P. syringae* produces
466 coronatine, a phytotoxin that mimics JA-Ile and acts by inhibiting the accumulation of
467 SA in order to promote bacterial growth (Zheng *et al*., 2012). Conversely, in
468 *Arabidopsis*, coronatine-insensitive mutants that are resistant to *Pst* display higher
469 levels of SA (Block *et al*., 2005). In *Arabidopsis*, the SA and JA pathways antagonize
470 each other (Li *et al*., 2019; Mur *et al*., 2006). However, JA pathway markers are also
471 down-regulated in response to d18:0/*Pst AvrRpm1* infiltration. Considering these
472 results, we could conceive that co-infiltration represses or does not activate both SA
473 and JA pathways in response to the avirulent bacterium because of a lowered bacterial
474 virulence, a decreased susceptibility, and/or an altered perception of the pathogen.
475 AvrRpm1, AvrB, and AvrPphB effectors all possess a consensus N-terminal
476 myristoylation sites which are required for full avirulence function (Nimchuk *et al*.,
477 2000). Myristoylation process occurs inside the plant cell (Nimchuk *et al*., 2000) and is

478 catalyzed by NMT (*N*-myristoyltransferase) enzymes (Pierre *et al*., 2007). Here, *NMT1*
479 expression is significantly reduced at 24 and 48 hpi when *Pst* AvrRpm1 is co-infiltrated
480 with d18:0. d18:0 co-infiltration could thus interfere with the myristoylation of these
481 effectors. As a consequence, it prevents them from being redirected to the PM where
482 their targets are and consequently preventing their activity in *Arabidopsis*. Recently, a
483 mis-localization of RPM1 at the PM, due to a depletion in anionic phospholipids in the
484 PM, inhibits its cell death activity (Saile *et al*., 2021). Since cell death is still induced,
485 such depletion does not affect RPS5 function, which is constitutively PM localized due
486 to the presence of myristoylation motifs in its sequence. RPS5 mediates the recognition
487 of AvrPphB. Co-infiltration of this effector with d18:0 results in an absence of HR, thus
488 excluding the involvement of a PM phospholipid dependent mechanism. PM
489 localization and stability of NLRs is essential for their activity in the induction of cell
490 death and immune responses (Saile *et al*., 2021). Effector localization into plant cell is
491 also essential for their interaction with their targets and subsequent activity (Nimchuk
492 *et al*., 2000). The inability for AvrRPM1 to interact with its target implies not only that
493 all the downstream plant defense responses are not activated but also the absence of
494 RPM1 degradation after co-infiltration. Moreover, mutation of consensus myristoylation
495 sites of *AvrRPM1* or *AvrB* leads to a highly reduction of HR events and an unhindered
496 pathogen growth (Nimchuk *et al*., 2000), consistent with our results.
497 All the effects of d18:0 previously mentioned, and its amphiphilic nature suggest that
498 the molecule can interact with the plant PM. It was thus hypothesized that it could insert
499 into the lipid fraction of the PM, as already suggested for other molecules such as fatty
500 acid hydroperoxides, rhamnolipids, lipopeptides that interact with lipids of plant PMs
501 (Cordelier *et al*., 2022; Deboever *et al*., 2022; Deleu *et al*., 2013, 2008; Henry *et al*.,
502 2011; Nasir *et al*., 2010; Schellenberger *et al*., 2021). Here, biophysical studies have

503 shown that d18:0 was attracted by, interacted with and stayed in biomimetic plant PMs.
504 These findings were further supported by *in silico* and *in vitro* analyses as well as
505 microscopic observations that notably showed d18:0 could disturb the lateral
506 organization and mechanical properties of plant PM and more specifically of its
507 microdomains. While it was suggested that exogenous LCB could cross the PM by
508 passive diffusion (Glenz *et al*., 2019), our results suggested that d18:0 has no
509 propensity to go into the intracellular medium. It actually possesses a flip-flop potential
510 within the PM meaning that exogenous addition of d18:0 could disturb the PM. As
511 previously stated, this interaction could eventually disturb defense-related proteins
512 located within its domains (Gronnier *et al*., 2018, 2016; Huby *et al*., 2020; Mamode
513 Cassim *et al*., 2019; Nagano *et al*., 2016), which could explain the absence of
514 extracellular ROS production observed in response to *Pst*. Lipid composition and
515 organization of the PM influence PM localization and stability of NLRs and
516 consequently their activity in cell death inducing (Saile *et al*., 2021). By disturbing the
517 PM organization, exogenous addition of d18:0 could also influence NLR localization
518 and function.
519 Collectively, our results demonstrated that d18:0 could have a dual effect on the PM
520 when co-infiltrated with *Pst AvrRpm1* by disturbing the organization and mechanical
521 properties of the PM and the myristoylation process, and thus the redirection of
522 effectors to the PM. Both actions prevent the interactions of NLR with its effector and
523 subsequent defense responses.
524

525 **MATERIAL AND METHODS**

526 **Plant material and growth conditions**

527 Seeds of the *Arabidopsis* T-DNA insertion mutants *rpm1-3* (CS68739), *rpm1-rps2-rin4*
528 (CS68760), and transgenic line *RPM1-myc rpm1* (CS68778) were obtained from the

529 Nottingham *Arabidopsis* Stock Center (http://Arabidopsis.info). Mutants, transgenic lines and
530 wild-type seeds Columbia-0 (Col-0) were grown in soil under 12 h-light/12 h-dark conditions
531 (150 µmol/m^2/s, 20°C, and 60% humidity) for 5 weeks.
532
533 **Chemicals**
534 Sphinganine (d18:0), palmitoyl-2-linoleoyl-*sn*-glycero-3-phosphocholine (PLPC), sitosterol
535 (sito), *D*-glucosyl-ß-1,1′-*N*-palmitoyl-*D*-erythro-sphingosine (d18:1/16:0 - GluCer or
536 Glucosylceramide) were purchased from Avanti Polar Lipids. Sphingolipids were dissolved in
537 ethanol (100%); PLPC, sitosterol and GluCer were dissolved in chloroform/methanol (2:1, v:v),
538 and used without further purification. Protamine sulphate was purchased from Sigma-Aldrich
539 (France).
540
541 **Bacterial cultures and inoculations**
542 *Pst* DC3000 strains transformed to express the effectors AvrRpm1 (*Pst AvrRpm1*), AvrRpt2
543 (*Pst AvrRpt2*), AvrRps4 (*Pst AvrRps4*), AvrB (*Pst AvrB*) or AvrPphB (*Pst AvrPphB*) were
544 provided by Prof. Jeff Dangl (University of North Carolina, USA) and Dr. Farid El-Kasmi
545 (University of Tübingen, Germany), Prof. Brian Staskawicz (University of California, USA),
546 Prof. Jane Parker (Max-Planck Institute, Cologne, Germany) and Dr. Brad Day (Michigan State
547 university, USA), respectively. Bacteria were cultured overnight under agitation (180 rpm) at
548 28°C in liquid King's B medium, supplemented with rifampicin (50 µg/mL) and kanamycin (50
549 µg/mL). Bacterial cells were collected by centrifugation, washed twice, and resuspended in 10
550 mM $MgCl_2$. Bacterial solutions were infiltrated at 10^7 CFU/mL on the abaxial side of *Arabidopsis*
551 leaves using a 1 mL syringe without needle. Co-treatment of bacteria with 100 µM d18:0 was
552 performed likewise. Control inoculations were conducted with 10 mM $MgCl_2$. At least four
553 leaves per plant were treated for each condition, with a minimum of three different plants.
554
555 ***In vitro* antibacterial assays**

556 Bacteria were cultured as previously described before being distributed in 96 wells plates at
557 10^7 CFU/mL in King's B medium supplemented with appropriate antibiotics, under agitation
558 and at 28°C. Bacteria were plated either alone, with ethanol (0.1%, v/v) or with d18:0 (100 µM).
559 OD_{600} measurements were performed using the TECAN Spark® (USA) absorbance reader,
560 every hour for 50 h. The presented data are obtained from growth curve experiments, from
561 which the growth rate was extracted.
562
563 **Pathogen assay *in planta***
564 For bacterial count experiments, bacterial cells were cultured and inoculated as described.
565 Four inoculated leaves were weighed and ground in 1 mL of 10 mM $MgCl_2$ using a mortar and
566 pestle. Appropriate dilutions were plated on King's B medium with suitable antibiotics, and
567 bacterial colonies were counted. Data are reported as means ±SD of the log (CFU/mg fresh
568 weight) of three replicates.
569
570 **RNA extraction and qRT-PCR**
571 Isolation of total RNA and real-time PCR were performed as described by Magnin-Robert et
572 al. (2015). Gene-specific primers are available in the Supplemental Table S1. For each
573 experiment, PCR was performed in triplicates. Transcript levels were normalized against those
574 of the UBIQUITIN5 (*UBQ5*) gene, used as an internal control. Fold induction compared with
575 untreated sample was calculated using the $2^{-\Delta\Delta Ct}$ method, where $\Delta\Delta Ct=$
576 $(Ct_{GI[unknown\ sample]}-Ct_{GI[reference\ sample]})-(Ct_{UBQ5[unknown\ sample]}-Ct_{UBQ5[reference\ sample]})$ where GI is the gene
577 of interest.
578
579 **Immunoblotting assay**
580 Total proteins from pre-treated leaves of *RPM1-myc rpm1* plants collected 0, 2, 6 and 24 hpi
581 were extracted and western-blotted according to Luzuriaga-Loaiza *et al*. (2018). Membrane
582 hybridization was carried out through overnight incubation with recombinant monoclonal Anti-
583 c-myc epitope tag [Clone 9E10] Mouse IgG1 kappa (Cliniscience, 1:1000) at 4°C, followed by

584 a 1 h incubation with anti-mouse IgG HRP-conjugated secondary antibodies (Bio-Rad, 1:3000)
585 at room temperature.
586
587 **Electrolyte leakage**
588 Measurement of electrolyte leakage were performed as described in Magnin-Robert *et al*.
589 (2015), except for leaf discs placed in each well of a 24-well plate containing 1 mL of distilled
590 water. Conductivity measurements were then conducted over time using a B-771 LaquaTwin
591 (Horiba) conductivity meter.
592
593 **Extracellular ROS production**
594 Measurements of extracellular ROS production were performed as described in Magnin-Robert
595 *et al*. (2015). Bacteria were added to a final concentration of 10^8 or 10^9 CFU/mL, as specified
596 further. In tests involving d18:0, the molecule was added at a final concentration of 100 µM
597 concomitantly with the elicitation solution.
598
599 **Phytohormone and camalexin quantifications**
600 The quantification of SA, JA-isoleucine (JA-Ile) and camalexin was performed at 0 and 48 hpi
601 by UPLC-nano-ESI-MS/MS as previously described in Herrfurth *et al*. (2020). Phytohormones
602 were extracted with methyl-tert-butyl ether (MTBE), reversed phase-separated using an
603 ACQUITY UPLC® system (Waters Corp., USA) and analysed by nanoelectrospray ionization
604 (nanoESI) (TriVersa Nanomate®; Advion BioSciences, USA) coupled with an AB Sciex 4000
605 QTRAP® tandem mass spectrometer (AB Sciex, USA) employed in scheduled multiple
606 reaction monitoring mode. For quantification, 10 ng D_4-SA (C/D/N Isotopes Inc., Canada),
607 20 ng D_5-IAA (Eurisotop, Germany), and 10 ng D_3-JA-Leu (kindly provided by Otto Miersch,
608 Halle/Saale, Germany) were added at the beginning of the extraction procedure. For detection,
609 the following mass transitions were used: 137/93 (declustering potential (DP) −25 V, entrance
610 potential (EP) -6 V, collision energy (CE) −20 V) for SA, 141/97 (DP −25 V, EP −6 V, CE −22
611 V) for D_4-SA, 179/135 (DP −35 V, EP −9 V, CE -14 V) for D_5-indole-acetic acid, 199/141 (DP

612 −60 V, EP −4 V, CE -32 V) for camalexin, 322/130 (DP −45 V, EP −5 V, CE -28 V) for JA-Ile
613 and 325/133 (DP −65 V, EP −4 V, CE -30 V) for D_3-JA-Leu.
614
615 **GUS reporter assays**
616 To determine induction of *PR1*, GUS enzyme activity of *PR1::GUS Arabidopsis* plants was
617 determined histochemically on leaves of the reporter line, treated as previously described,
618 collected at 48 hpi, and placed in the GUS staining solution (50 mM sodium phosphate buffer
619 - pH 7, 10mM EDTA, 1 mM $K_3Fe(CN)6$, 2 mM X-GlcA, and 0,1% Triton X-100). The leaves
620 were vacuum-infiltrated for 5 min and incubated for 4 h at 37°C. Next, they were washed with
621 Milli-Q water and left overnight at 4°C in a discoloration / fixation solution (ethanol:acetic acid,
622 3:1). Once the discoloration process was complete, leaves were placed in 95% (v/v) ethanol.
623
624 **Lipid composition for plant biomimetic membranes**
625 To mimic the lipid composition of plant PM, PLPC, β-sitosterol and GluCer were used, either
626 in a mixture (60:20:20, molar ratio) or alone, depending on the experiment. This lipid
627 composition was previously used to mimic plant PM (Deleu *et al*., 2014, 2019; Deboever *et al*.,
628 2022).
629
630 **Adsorption of sphinganine onto lipid monolayers using Langmuir trough**
631 Adsorption experiments at constant surface area were performed in a KSV (Helsinki, Finland)
632 Minitrough (190 cm^3) equipped with a Wilhelmy plate, as previously described (Nasir *et al*.,
633 2016; Deleu *et al.*, 2019). The maximal insertion pressure (MIP) and the differential Π_0 ($d\Pi_0$)
634 were determined as previously described (Deboever *et al*., 2020).
635
636 **Preparation of large unilamellar vesicles**

637 PLPC/ β-sitosterol/GluCer (60:20:20 molar ratio) large unilamellar vesicles (LUVs) were
638 prepared as described previously (Lebecque et al., 2019). Tris-HCl buffer (10 mM, pH 7.4) was
639 used for lipid film hydration and dispersion.
640 Extrusion was done *via* 13 passages through a 0.1 µM membrane filter using Liposofast
641 extruder (AVESTIN®). Diameter and stability of the LUVs were confirmed by dynamic light
642 scattering (DLS) measurements.
643
644 **Thermodynamic parameters of sphinganine interaction with lipid bilayers by isothermal**
645 **titration calorimetry**
646 For isothermal titration calorimetry (ITC) measurements, LUVs were prepared as described
647 and resuspended to reach a final concentration of 1 mM in Tris-HCl buffer (10 mM, pH 7.4).
648 Experiments were performed on a A VP-ITC microcalorimeter (Microcal Inc., Northampton,
649 MA, USA) as previously described (Lebecque *et al*., 2018). Details can be found in supporting
650 information section (Supplemental Material S1).
651
652 **Laurdan polarization on lipid vesicles LUVs**
653 LUVs suspension at a concentration of 100 µM in lipids was incubated with 1 µM of Laurdan
654 (Sigma-Aldrich) for 1h15. Then, wells of black 96-well microplates (Greiner Bio-
655 One™ CellStar™, Fischer Scientific) were loaded with 100 µL of liposome solution per well.
656 The fluorescence was recorded using Spark® microplate reader (Tecan) with an excitation
657 wavelength at 360 (±35) nm and emission wavelengths at 430 (±20) nm and 485 (±20) nm.
658 The fluorescence was recorded once before treatment and every 5 min for up to 20 minutes,
659 after the addition of 100 µL of 2-times concentrated treatment.
660 The generalized polarization (GP) was defined as GP = $\frac{(I_{430nm}-I_{485nm})}{(I_{430nm}+I_{485nm})}$, where I_{430nm} and I_{485nm}
661 represents the blank-subtracted fluorescence intensities at emission wavelengths of 430 nm
662 and 485 nm respectively. Variation of GP (ΔGP) is defined as the subtraction of GP measured
663 at each time point following treatment from GP measured before treatment.

664

665 **Propensity of sphinganine to insert into a bilayer determined by the Impala procedure**

666 The most energetically favorable position and orientation of d18:0 in an implicite lipid bilayer
667 was determined with the same procedure described in Ducarme *et al*. (1998) and Franche *et*
668 *al*. (2020). For more details, see Supplementary Material S1.

669

670 **Interaction energies between sphinganine and lipids determined by the Hypermatrix**
671 **docking method**

672 The hypermatrix docking method was employed, as previously described (Deleu *et al*., 2014;
673 Deleu *et al*., 2019) to dock a molecule of sphinganine to a lipid system composed of either
674 plant or bacterial lipids.

675

676 **Modeling of sphinganine/plant lipids monolayer interactions with Big Monolayer**
677 **method**

678 The big monolayer method, as described by Deleu *et al.* (2019), was used to visualize lipid
679 domains. Three repetitions of the system were calculated. The simulations were performed
680 using plant lipid mixture with or without d18:0 (88% lipids, 12% d18:0).

681

682 **Protoplast isolation**

683 The isolation of mesophyll protoplasts was carried out by an enzymatic method as previously
684 described (Yoo *et al*., 2007). The protoplasts were resuspended at 10^6 protoplasts/mL in a
685 storage solution (20 mM MES, 400 mM mannitol, 20 mM KCl, 10 mM $CaCl_2$) until further use.

686

687 **Atomic force microscopy**

688 Protoplasts were adhered to the bottom of a glass-bottom Petrie dish by coating with positive-
689 charge-bearing protamine sulphate 1 % in water: the bottom of the Petri dish was covered with
690 a thin layer of this solution during 2 min, rinsed 3 times with the protoplast storage solution and
691 the remaining solution was discarded. Protoplast suspension was incubated for 5 min with final

692 concentration 2 µM or 5 µM of d18:0 or control ethanol in protoplasts storage solution for 5
693 min. Then, pre-treated or not protoplasts suspension was gently deposited to the coating Petri
694 dish, and the protoplasts were settled for 5 min.
695 QNM-LC-CAL probes (Bruker, Billerica, USA), having a resonance frequency of 45 kHz, a tip
696 radius of 65 nm, a tip height of 16 µm and a nominal spring constant below 100 mN/m were
697 calibrated on a non-compliant sample to extract the deflection sensitivity which turned out to
698 be around 10 nm/V. Afterwards the tip was pulled off (of 100 Um) and tuned in liquid to
699 determine the spring constant.
700 Optics (Nikon Ti 2000, Nikon, Tokyo, Japan) were used in bright field mode to browse through
701 all protoplasts and focus on those having a 100 µm diameter. Therefore, the tip was engaged
702 at the very center of each and forces curves were captured in single force spectroscopy mode.
703 The atomic force microscopy (AFM) used was a Bioscope Catalyst (Bruker, Billerica, USA). A
704 z ramp output was used, with a ramp size of 5 µm, a ramp rate of 0.25 Hz, a contact time of
705 50 msec, and a forward and backward velocities of 5 µm/sec. Each force curves contained
706 2048 points. The Poisson's ratio was arbitrary set at 0.3. We used a relative trigger mode, a
707 tip threshold of 30 nm and plotted the deflection error as data type. It was verified that there
708 was no apparent change in diameter or x,y motion of the object during the acquisition.
709 The Young's modulus was extracted according to the Hert's theory and normalized as a
710 function of the protoplasts' volumes. A minimum of 50 curves per condition were recorded and
711 experiments were repeated three times.
712
713 **Confocal microscopy**
714 To determine the membrane order, protoplasts were labelled with 300 nM final concentration
715 of fluorescent probe di-4-ANEPPDHQ (Invitrogen, stock solution 1.5 mM in DMSO) in
716 protoplast storage solution, during 5 min. The labelled protoplasts suspension was gently
717 deposited to the bottom of a glass bottom Petri dish and the protoplasts were settled for 5 min.
718 The labelled protoplast suspension was incubated for 5 min with final concentration 2 µM or 5
719 µM of d18:0 or control ethanol for 5 min.

720 Fluorescence images were acquired using a laser scanning microscope LSM 880 from ZEISS
721 (Carl ZEISS SAS, Rueil Malmaison, France) through 63x (ON 1.4) oil immersion objective with
722 ZEN software. Di-4-ANEPPDHQ excitation was done at 488 nm and emission intensities were
723 acquired between 540–560 nm (green image) and between 630–650 nm (red image).
724 Ratiometric imaging was performed using the Fiji software (Schindelin *et al*., 2021).
725

726 **ACKNOWLEDGEMENT**

727 The authors thank Prof. Jeff Dangl (University of North Carolina, USA), Dr. Farid El-Kasmi
728 (University of Tübingen, Germany), Prof. Brian Staskawicz (University of California, USA),
729 Prof. Jane Parker (Max-Planck Institute, Cologne, Germany) and Dr. Brad Day (Michigan State
730 university, USA) for generously providing the different bacterial strains used in this study.
731 This work was supported by the National Fund for Scientific Research (FNRS, Belgium), the
732 SFR Condorcet (18ARC107), and the "Fondation Universitaire de Belgique" (Belgian
733 University Foundation). Some of the experiments were carried out within the Nanomat platform
734 (www.nanomat.eu) supported by the Ministère de l'Enseignement Supérieur et de la
735 Recherche, the Région Grand Est, and FEDER funds from the European Community. GG was
736 supported by the Foundation for Training in Industrial and Agricultural Research (FRIA, FNRS,
737 grant 1.E.069.20F), and MD is Senior Research Associates of the FNRS. I.F. acknowledges
738 funding by the Deutsche Forschungsgemeinschaft (INST 186/822-1).
739

740 **AUTHOR CONTRIBUTIONS**

741 SDC and MD designed the research. EH, SV, AB, CT, CCh, CH and GG performed
742 the research. EH, MD, SDC, FB analyzed and discussed the data. SC, SD, JC, CJ, FF,
743 CCl, IF provided critical feedback on the manuscript. EH, MD and SDC wrote the paper
744 and incorporated the input of the rest of the authors.
745

746 **SUPPLEMENTAL DATA**

747 **Supplemental Figure S1.** Adsorption behaviour of d18:0 into lipid
748 monolayer mimicking plant plasma membrane

749 **Supplemental Table S1.** Gene-specific primers used in real-time reverse transcription
750 PCR.

751 **Supplementary Material S1**. Methods in biophysics.

752

753 **Conflict of interest statement**

754 The authors declare no conflict of interest.

755

756 **Orcid**

757 Sylvain Cordelier: https://orcid.org/0000-0001-7723-4145
758 Jérôme Crouzet: https://orcid.org/0000-0003-0458-830X
759 Magali Deleu: https://orcid.org/0000-0001-8255-2965
760 Sandrine Dhondt-Cordelier: https://orcid.org/0000-0002-3778-6727
761 Stéphan Dorey: https://orcid.org/0000-0002-9583-2824
762 Ivo Feussner: https://orcid.org/0000-0002-9888-7003
763 Florence Fontaine: https://orcid.org/ 0000-0003-2918-8812
764 Guillaume Gilliard: https://orcid.org/0000-0002-4651-2920
765 Cornelia Herrfurth: https://orcid.org/0000-0001-8255-3255
766 Cédric Jacquard: https//orcid.org/0000-0003-4284-6082
767

768 **References**

769 Ade, J., DeYoung, B.J., Golstein, C., Innes, R.W., 2007. Indirect activation of a plant nucleotide binding
770 site-leucine-rich repeat protein by a bacterial protease. Proceedings of the National Academy of
771 Sciences U.S.A. 104, 2531–2536.
772 Ali, U., Li, H., Wang, X., Guo, L., 2018. Emerging roles of sphingolipid signaling in plant response to
773 biotic and abiotic stresses. Molecular Plant 11, 1328–1343.
774 Bari, R., Jones, J.D.G., 2009. Role of plant hormones in plant defence responses. Plant Molecular
775 Biology 69, 473–488.
776 Berkey, R., Bendigeri, D., Xiao, S., 2012. Sphingolipids and Plant Defense/Disease: The "Death"
777 Connection and Beyond. Frontiers in Plant Science 3.
778 Betsuyaku, S., Katou, S., Takebayashi, Y., Sakakibara, H., Nomura, N., Fukuda, H., 2018. Salicylic Acid
779 and Jasmonic Acid Pathways are Activated in Spatially Different Domains Around the Infection Site
780 During Effector-Triggered Immunity in *Arabidopsis thaliana*. Plant and Cell Physiology 59, 8–16.
781 Bjornson, M., Zipfel, C., 2021. Plant immunity: Crosstalk between plant immune receptors. Current
782 Biology 31, R796–R798.
783 Block, A., Schmelz, E., Jones, J.B., Klee, H.J., 2005. Coronatine and salicylic acid: the battle between
784 *Arabidopsis* and *Pseudomonas* for phytohormone control. Molecular Plant Pathology 6, 79–83.
785 Boyes, D.C., Nam, J., Dangl, J.L., 1998. The *Arabidopsis thaliana* RPM1 disease resistance gene
786 product is a peripheral plasma membrane protein that is degraded coincident with the hypersensitive
787 response. Proceedings of the National Academy of Sciences U.S.A. 95, 15849–15854.
788 Boyle, P.C., Martin, G.B., 2015. Greasy tactics in the plant-pathogen molecular arms race. Journal of
789 Experimental Botany 66, 1607–1616.
790 Brasseur, R., Killian, J.A., De Kruijff, B., Ruysschaert, J.M., 1987. Conformational analysis of gramicidin-
791 gramicidin interactions at the air/water interface suggests that gramicidin aggregates into tube-like
792 structures similar as found in the gramicidin-induced hexagonal HII phase. Biochimica et Biophysica
793 Acta (BBA) - Biomembranes 903, 11–17.
794 Brooks, D.M., Bender, C.L., Kunkel, B.N., 2005. The *Pseudomonas syringae* phytotoxin coronatine
795 promotes virulence by overcoming salicylic acid-dependent defences in *Arabidopsis thaliana*.
796 Molecular Plant Pathology 6, 629–639.

Buell, C.R., Joardar, V., Lindeberg, M., Selengut, J., Paulsen, I.T., Gwinn, M.L., Dodson, R.J., Deboy, R.T., Durkin, A.S., Kolonay, J.F., Madupu, R., Daugherty, S., Brinkac, L., Beanan, M.J., Haft, D.H., Nelson, W.C., Davidsen, T., Zafar, N., Zhou, L., Liu, J., Yuan, Q., Khouri, H., Fedorova, N., Tran, B., Russell, D., Berry, K., Utterback, T., Van Aken, S.E., Feldblyum, T.V., D'Ascenzo, M., Deng, W.-L., Ramos, A.R., Alfano, J.R., Cartinhour, S., Chatterjee, A.K., Delaney, T.P., Lazarowitz, S.G., Martin, G.B., Schneider, D.J., Tang, X., Bender, C.L., White, O., Fraser, C.M., Collmer, A., 2003. The complete genome sequence of the *Arabidopsis* and tomato pathogen *Pseudomonas syringae* pv. *tomato* DC3000. Proceedings of the National Academy of Sciences U.S.A. 100, 10181–10186.

Cacas, J.-L., Buré, C., Grosjean, K., Gerbeau-Pissot, P., Lherminier, J., Rombouts, Y., Maes, E., Bossard, C., Gronnier, J., Furt, F., Fouillen, L., Germain, V., Bayer, E., Cluzet, S., Robert, F., Schmitter, J.-M., Deleu, M., Lins, L., Simon-Plas, F., Mongrand, S., 2016. Revisiting plant plasma membrane lipids in tobacco: A focus on sphingolipids. Plant Physiology 170, 367–384.

Chen, M., Markham, J.E., Dietrich, C.R., Jaworski, J.G., Cahoon, E.B., 2008. Sphingolipid long-chain base hydroxylation is important for growth and regulation of sphingolipid content and composition in *Arabidopsis*. The Plant Cell 20, 1862–1878.

Contreras, F.-X., Sot, J., Alonso, A., Goñi, F.M., 2006. Sphingosine Increases the Permeability of Model and Cell Membranes. Biophysical Journal 90, 4085–4092.

Cordelier, S., Crouzet, J., Gilliard, G., Dorey, S., Deleu, M., Dhondt-Cordelier, S., 2022. Deciphering the role of plant plasma membrane lipids in response to invasion patterns: how could biology and biophysics help? Journal of Experimental Botany 73, 2765-2784.

Coursol, S., Fromentin, J., Noirot, E., Brière, C., Robert, F., Morel, J., Liang, Y.-K., Lherminier, J. and Simon-Plas, F., 2015. Long-chain bases and their phosphorylated derivatives differentially regulate cryptogein-induced production of reactive oxygen species in tobacco (*Nicotiana tabacum*) BY-2 cells. New Phytologist 205: 1239-1249.

Couto, D., Zipfel, C., 2016. Regulation of pattern recognition receptor signalling in plants. Nature Review Immunology 16, 537–552.

Debener, T., Lehnackers, H., Arnold, M., Dangl, J.L., 1991. Identification and molecular mapping of a single *Arabidopsis thaliana* locus determining resistance to a phytopathogenic *Pseudomonas syringae* isolate. The Plant Journal 1, 289–302.

Deboever, E., Lins L, Ongena M, De Clerck C, Deleu M, Fauconnier ML. 2020. Linolenic fatty acid hydroperoxide acts as biocide on plant pathogenic bacteria: Biophysical investigation of the mode of action. Bioorganic Chemistry 100, 10387.

Deboever, E., Van Aubel, G., Rondelli, V., Koutsioubas, A., Mathelie-Guinlet, M., Dufrene, Y.F., Ongena, M., Lins, L., Van Cutsem, P., Fauconnier, M., Deleu, M., 2022. Modulation of plant plasma membrane structure by exogenous fatty acid hydroperoxide is a potential perception mechanism for their eliciting activity. Plant Cell & Environment 45, 1082–1095.

Deleu, M., Crowet, J.-M., Nasir, M.N., Lins, L., 2014. Complementary biophysical tools to investigate lipid specificity in the interaction between bioactive molecules and the plasma membrane: A review. Biochimica et Biophysica Acta (BBA) - Biomembranes 1838, 3171–3190.

Deleu, M., Deboever, E., Nasir, M.N., Crowet, J.-M., Dauchez, M., Ongena, M., Jijakli, H., Fauconnier, M.-L., Lins, L., 2019. Linoleic and linolenic acid hydroperoxides interact differentially with biomimetic plant membranes in a lipid specific manner. Colloids and Surfaces B: Biointerfaces 175, 384–391.

Deleu, M., Lorent, J., Lins, L., Brasseur, R., Braun, N., El Kirat, K., Nylander, T., Dufrêne, Y.F., Mingeot-Leclercq, M.-P., 2013. Effects of surfactin on membrane models displaying lipid phase separation. Biochimica et Biophysica Acta (BBA) - Biomembranes 1828, 801–815.

Deleu, M., Paquot, M., Nylander, T., 2008. Effect of Fengycin, a Lipopeptide Produced by *Bacillus subtilis*, on Model Biomembranes. Biophysical Journal 94, 2667–2679.

Desveaux, D., Singer, AU., Dangl JL., 2006. Type III effector proteins: doppelgangers of bacterial virulence. Current Opinion in Plant Biology 9, 376-382.

Dinic, J., Biverståhl, H., Mäler, L., Parmryd, I., 2011. Laurdan and di-4-ANEPPDHQ do not respond to membrane-inserted peptides and are good probes for lipid packing. Biochimica Biophysica Acta 1808, 298–306.

Dodds, P.N., Rafiqi, M., Gan, P.H.P., Hardham, A.R., Jones, D.A. and Ellis, J.G. (2009), Effectors of biotrophic fungi and oomycetes: pathogenicity factors and triggers of host resistance. New Phytologist, 183: 993-1000.

Ducarme, P., Rahman, M., Brasseur, R., 1998. IMPALA: A simple restraint field to simulate the biological membrane in molecular structure studies. PROTEINS: Structure, Function, and Genetics 30:357–371

Fischer, C.L., Drake, D.R., Dawson, D.V., Blanchette, D.R., Brogden, K.A., Wertz, P.W., 2012. Antibacterial activity of sphingoid bases and fatty acids against gram-positive and gram-negative bacteria. Antimicrobial Agents and Chemotherapy 56, 1157–1161.

857 Franche, A., Fayeulle, A., Lins, L., Billamboz, M., Pezron, I., Deleu, M., Léonard, E., 2020. Amphiphilic
858 azobenzenes: Antibacterial activities and biophysical investigation of their interaction with bacterial
859 membrane lipids. Bioorganic Chemistry 94, 103399.
860 Furlan, A.L., Laurin, Y., Botcazon, C., Rodríguez-Moraga, N., Rippa, S., Deleu, M., Lins, L., Sarazin, C.,
861 Buchoux, S., 2020. Contributions and limitations of biophysical approaches to study of the interactions
862 between amphiphilic molecules and the plant plasma membrane. Plants 9, 648.
863 Gassmann, W., Hinsch, M.E., Staskawicz, B.J., 1999. The *Arabidopsis* RPS4 bacterial-resistance gene
864 is a member of the TIR-NBS-LRR family of disease-resistance genes. The Plant Journal 20, 265–277.
865 Gerbeau-Pissot, P., Der, C., Thomas, D., Anca, I.-A., Grosjean, K., Roche, Y., Perrier-Cornet, J.-M.,
866 Mongrand, S., Simon-Plas, F., 2014. Modification of plasma membrane organization in tobacco cells
867 elicited by cryptogein. Plant Physiology 164, 273–286.
868 Glenz, R., Kaiping, A., Göpfert, D., Weber, H., Lambour, B., Sylvester, M., Fröschel, C., Mueller, M.J.,
869 Osman, M., Waller, F., 2022. The major plant sphingolipid long chain base phytosphingosine inhibits
870 growth of bacterial and fungal plant pathogens. Scientific Reports 12, 1081.
871 Glenz, R., Schmalhaus, D., Krischke, M., Mueller, M.J., Waller, F., 2019. Elevated levels of
872 phosphorylated sphingobases do not antagonize sphingobase- or fumonisin B1-induced plant cell
873 death. Plant and Cell Physiology 60, 1109–1119.
874 Grant, M., Godiard, L., Straube, E., Ashfield, T., Lewald, J., Sattler, A., Innes, R., Dangl, J., 1995.
875 Structure of the *Arabidopsis* RPM1 gene enabling dual specificity disease resistance. Science 269,
876 843–846.
877 Grennan, A.K., 2007. Lipid Rafts in Plants. Plant Physiology 143, 1083–1085.
878 Gronnier, J., Gerbeau-Pissot, P., Germain, V., Mongrand, S., Simon-Plas, F., 2018. Divide and rule:
879 Plant plasma membrane organization. Trends in Plant Science 23, 899–917.
880 Gronnier, J., Germain, V., Gouguet, P., Cacas, J.-L., Mongrand, S., 2016. GIPC: Glycosyl Inositol
881 Phospho Ceramides, the major sphingolipids on earth. Plant Signaling & Behavior 11, e1152438.
882 Guan, R., Su, J., Meng, X., Li, S., Liu, Y., Xu, J., Zhang, S., 2015. Multilayered regulation of ethylene
883 induction plays a positive role in *Arabidopsis* resistance against *Pseudomonas syringae*. Plant
884 Physiology 169, 299–312.
885 Gutiérrez-Nájera, N.A., Saucedo-García, M., Noyola-Martínez, L., Vázquez-Vázquez, C., Palacios-
886 Bahena, S., Carmona-Salazar, L., Plasencia, J., El-Hafidi, M., Gavilanes-Ruiz, M., 2020. Sphingolipid
887 effects on the plasma membrane produced by addition of fumonisin B1 to maize embryos. Plants 9,
888 150.
889 Hao, H., Fan, L., Chen, T., Li, R., Li, X., He, Q., Botella, M.A., Lin, J., 2014. Clathrin and membrane
890 microdomains cooperatively regulate RbohD dynamics and activity in *Arabidopsis*. Plant Cell 26,
891 1729–1745.
892 Henry, E., Yadeta, K.A., Coaker, G., 2013. Recognition of bacterial plant pathogens: local, systemic and
893 transgenerational immunity. New Phytologist 199, 908–915.
894 Henry, G., Deleu, M., Jourdan, E., Thonart, P., Ongena, M., 2011, The bacterial lipopeptide surfactin
895 targets the lipid fraction of the plant plasma membrane to trigger immune-related defence responses.
896 Cellular Microbiology 13, 1824-1837.
897 Herrfurth, C., Feussner, I., 2020. Quantitative jasmonate profiling using a high-throughput UPLC-
898 NanoESI-MS/MS method. In: Champion, A., Laplaze, L. (eds) Jasmonate in Plant Biology. Methods
899 in Molecular Biology, vol 2085. Humana, New York, NY.
900 Hicks, S.W., Galán, J.E., 2013. Exploitation of eukaryotic subcellular targeting mechanisms by bacterial
901 effectors. Nature Reviews Microbiology 11, 316–326.
902 Huby, E., Napier, J.A., Baillieul, F., Michaelson, L.V., Dhondt-Cordelier, S., 2020. Sphingolipids: towards
903 an integrated view of metabolism during the plant stress response. New Phytologist 225, 659–670.
904 Ishikawa, T., Aki, T., Yanagisawa, S., Uchimiya, H., Kawai-Yamada, M., 2015. Overexpression of BAX
905 INHIBITOR-1 links plasma membrane microdomain proteins to stress. Plant Physiology 169, 1333–
906 1343.
907 Jones, J.D.G., Dangl, J.L., 2006. The plant immune system. Nature 444, 323–329.
908 Kadota, Y., Liebrand, T.W.H., Goto, Y., Sklenar, J., Derbyshire, P., Menke, F.L.H., Torres, M., Molina,
909 A., Zipfel, C., Coaker, G., Shirasu, K., 2019. Quantitative phosphoproteomic analysis reveals common
910 regulatory mechanisms between effector- and PAMP-triggered immunity in plants. New Phytologist
911 221, 2160–2175.
912 Kamoun, S., 2006. A catalogue of the effector secretome of plant pathogenic oomycetes. Annual Review
913 of Phytopathology 44, 41-60.
914 Kato, H., Nemoto, K., Shimizu, M., Abe, A., Asai, S., Ishihama, N., Matsuoka, S., Daimon, T., Ojika, M.,
915 Kawakita, K., Onai, K., Shirasu, K., Yoshida, M., Ishiura, M., Takemoto, D., Takano, Y., Terauchi, R.,
916 2022. Recognition of pathogen-derived sphingolipids in Arabidopsis, Science 376, 857-860.

Kawasaki, T., Nam, J., Boyes, D.C., Holt, B.F., Hubert, D.A., Wiig, A., Dangl, J.L., 2005. A duplicated pair of *Arabidopsis* RING-finger E3 ligases contribute to the RPM1- and RPS2-mediated hypersensitive response: Transmembrane RING-E3 ligases and the HR. The Plant Journal 44, 258–270.

Kimberlin, A.N., Han, G., Chen, M., Cahoon, R.E., Luttgeharm, K.D., Stone, J.M., Markham, J.E., Dunn, T.M., Cahoon, E.B., 2016. ORM expression alters sphingolipid homeostasis and differentially affects ceramide synthase activities. Plant Physiology 172, 889-900.

Klemptner, R.L., Sherwood, J.S., Tugizimana, F., Dubery, I.A., Piater, L.A., 2014. Ergosterol, an orphan fungal microbe-associated molecular pattern (MAMP): Ergosterol as a MAMP. Molecular Plant Pathology 15, 747–761.

König, S., Feussner, K., Schwarz, M., Kaever, A., Iven, T., Landesfeind, M., Ternes, P., Karlovsky, P., Lipka, V., Feussner, I., 2012. *Arabidopsis* mutants of sphingolipid fatty acid α-hydroxylases accumulate ceramides and salicylates. New Phytologist 196, 1086–1097.

König, S., Gömann, J., Zienkiewicz, A., Zienkiewicz, K., Meldau, D., Herrfurth, C., Feussner, I., 2021. Sphingolipid-induced programmed cell death is a salicylic acid and EDS1-dependent phenotype in *Arabidopsis*. Biochemistry 63, 317-325.

Lebecque, S., Crowet, J.-M., Lins, L., Delory, B.M., du Jardin, P., Fauconnier, M.-L., Deleu, M., 2018. Interaction between the barley allelochemical compounds gramine and hordenine and artificial lipid bilayers mimicking the plant plasma membrane. Scientific Reports 8, 9784.

Lee, C.C., Wood, M.D., Ng, K., Andersen, C.B., Liu, Y., Luginbühl, P., Spraggon, G., Katagiri, F., 2004. Crystal structure of the type III effector AvrB from *Pseudomonas syringae*. Structure 12, 487–494.

Lee, D., Bourdais, G., Yu, G., Robatzek, S., Coaker, G., 2015. Phosphorylation of the plant immune regulator RPM1-INTERACTING PROTEIN4 enhances plant plasma membrane H + -ATPase activity and inhibits flagellin-triggered immune responses in *Arabidopsis*. Plant Cell 27, 2042–2056.

Lenarčič, T., Albert, I., Böhm, H., Hodnik, V., Pirc, K., Zavec, A.B., Podobnik, M., Pahovnik, D., Žagar, E., Pruitt, R., Greimel, P., Yamaji-Hasegawa, A., Kobayashi, T., Zienkiewicz, A., Gömann, J., Mortimer, J.C., Fang, L., Mamode-Cassim, A., Deleu, M., Lins, L., Oecking, C., Feussner, I., Mongrand, S., Anderluh, G., Nürnberger, T., 2017. Eudicot plant-specific sphingolipids determine host selectivity of microbial NLP cytolysins. Science 358, 1431–1434.

Lherminier, J., Elmayan, T., Fromentin, J., Elaraqui, K.T., Vesa, S., Morel, J., Verrier, J.-L., Cailleteau, B., Blein, J.-P., Simon-Plas, F., 2009. NADPH oxidase-mediated reactive oxygen species production: Subcellular localization and reassessment of its role in plant defense. Molecular Plant-Microbe Interactions 22, 868–881.

Li, N., Han, X., Feng, D., Yuan, D., Huang, L.-J., 2019. Signaling crosstalk between salicylic acid and ethylene/jasmonate in plant defense: Do we understand what they are whispering? International Journal of Molecular Sciences 20, 671.

Luttgeharm, K.D., Kimberlin, A.N., Cahoon, E.B., 2016. Plant sphingolipid metabolism and function, in: Nakamura, Y., Li-Beisson, Y. (Eds.), Lipids in Plant and Algae Development. Springer International Publishing, Cham, pp. 249–286.

Luzuriaga-Loaiza, W.P., Schellenberger, R., De Gaetano, Y., Obounou Akong, F., Villaume, S., Crouzet, J., Haudrechy, A., Baillieul, F., Clément, C., Lins, L., Allais, F., Ongena, M., Bouquillon, S., Deleu, M., Dorey, S., 2018. Synthetic rhamnolipid bolaforms trigger an innate immune response in *Arabidopsis thaliana*. Scientific Reports 8, 8534.

Mackey, D., Belkhadir, Y., Alonso, J.M., Ecker, J.R., Dangl, J.L., 2003. *Arabidopsis* RIN4 is a target of the type III virulence effector AvrRpt2 and modulates RPS2-mediated resistance. Cell 112, 379–389.

Mackey, D., Holt III, B.F., Wiig, A., Dangl, J.L., 2002. RIN4 interacts with *Pseudomonas syringae* type III effector molecules and is required for RPM1-mediated resistance in *Arabidopsis*. Cell 108, 743–754.

Magazzù, A., Marcuello, C., 2023. Investigation of soft matter nanomechanics by atomic force microscopy and optical tweezers: A comprehensive review. Nanomaterials 13, 963.

Magnin-Robert, M., Le Bourse, D., Markham, J.E., Dorey, S., Clément, C., Baillieul, F., Dhondt-Cordelier, S., 2015. Modifications of sphingolipid content affect tolerance to hemibiotrophic and necrotrophic pathogens by modulating plant defense responses in *Arabidopsis*. Plant Physiology 169, 2255-2274.

Mamode Cassim, A., Gouguet, P., Gronnier, J., Laurent, N., Germain, V., Grison, M., Boutté, Y., Gerbeau-Pissot, P., Simon-Plas, F., Mongrand, S., 2019. Plant lipids: Key players of plasma membrane organization and function. Progress in Lipid Research 73, 1–27.

Marsh, D., 1996. Lateral pressure in membranes. Biochimica et Biophysica Acta (BBA) - Reviews on Biomembranes 1286, 183–223.

Mongrand, S., Morel, J., Laroche, J., Claverol, S., Carde, J.-P., Hartmann, M.-A., Bonneu, M., Simon-Plas, F., Lessire, R., Bessoule, J.-J., 2004. Lipid rafts in higher plant cells: purification and characterization of triton x-100-insoluble microdomains from tobacco plasma membrane. Journal Biological Chemistry 279, 36277–36286.

Moore, R.A., Starratt, A.N., Ma, S.-W., Morris, V.L., Cuppels, D.A., 1989. Identification of a chromosomal region required for biosynthesis of the phytotoxin coronatine by *Pseudomonas syringae* pv. tomato. Canadian Journal of Microbiology 35, 910–917.

Mur, L.A.J., Kenton, P., Atzorn, R., Miersch, O., Wasternack, C., 2006. The outcomes of concentration-specific interactions between salicylate and jasmonate signaling include synergy, antagonism, and oxidative stress leading to cell death. Plant Physiology 140, 249–262.

Nagano, M., Ishikawa, T., Fujiwara, M., Fukao, Y., Kawano, Y., Kawai-Yamada, M., Shimamoto, K., 2016. Plasma membrane microdomains are essential for Rac1-RbohB/H-mediated immunity in rice. The Plant Cell 28, 1966–1983.

Nasir, M.N., Crowet, J.-M., Lins, L., Obounou Akong, F., Haudrechy, A., Bouquillon, S., Deleu, M., 2016. Interactions of sugar-based bolaamphiphiles with biomimetic systems of plasma membranes. Biochimie 130, 23–32.

Nasir, M.N., Thawani, A., Kouzayha, A., Besson, F., 2010. Interactions of the natural antimicrobial mycosubtilin with phospholipid membrane models. Colloids and Surfaces B: Biointerfaces 78, 17–23.

Ngou, B.P.M., Ahn, H.-K., Ding, P., Jones, J.D.G., 2021. Mutual potentiation of plant immunity by cell-surface and intracellular receptors. Nature 592, 110–115.

Nimchuk, Z., Marois, E., Kjemtrup, S., Leister, R.T., Katagiri, F., Dangl, J.L., 2000. Eukaryotic fatty acylation drives plasma membrane targeting and enhances function of several type III effector proteins from *Pseudomonas syringae*. Cell 101, 353–363.

Parasassi, T., De Stasio, G., Ravagnan, G., Rusch, R.M., Gratton, E., 1991. Quantitation of lipid phases in phospholipid vesicles by the generalized polarization of Laurdan fluorescence. Biophysical Journal 60, 179–189.

Pata, M.O., Hannun, Y.A., Ng, C.K.-Y., 2010. Plant sphingolipids: decoding the enigma of the Sphinx: Tansley review. New Phytologist 185, 611–630.

Peer, M., Bach, M., Mueller, M.J., Waller, F., 2011. Free sphingobases induce RBOHD-dependent reactive oxygen species production in *Arabidopsis* leaves. FEBS Letters 585, 3006–3010.

Pierre M., Traverso J.A., Boisson B., Domenichini S., Bouchez D., Giglione C., Meinnel T., 2007. *N*-myristoylation regulates the SnRK1 pathway in *Arabidopsis*, The Plant Cell 19, 2804–2821

Pottinger, S.E., Innes, R.W., 2020. RPS5-Mediated Disease Resistance: Fundamental Insights and Translational Applications. Annual Review of Phytopathology 58, 139-160.

Rondelli, V., Mollica, L., Koutsioubas, A., Nasir, N., Trapp, M., Deboever, E., Brocca, P., Deleu, M., 2022. Carbohydrate-carbohydrate interaction drives the preferential insertion of dirhamnolipid into glycosphingolipid enriched membranes. Journal of Colloid and Interface Science, 616, 739-748.

Rossard, S., Roblin, G., Atanassova, R., 2010. Ergosterol triggers characteristic elicitation steps in Beta vulgaris leaf tissues. Journal of Experimental Botany 61, 1807–1816.

Saijo, Y., Loo, E.P. iian, 2020. Plant immunity in signal integration between biotic and abiotic stress responses. New Phytologist 225, 87–104.

Saile, S.C., Ackermann, F.M., Sunil, S., Keicher, J., Bayless, A., Bonardi, V., Wan, L., Doumane, M., Stöbbe, E., Jaillais, Y., Caillaud, M.-C., Dangl, J.L., Nishimura, M.T., Oecking, C. and El Kasmi, F. 2021. Arabidopsis ADR1 helper NLR immune receptors localize and function at the plasma membrane in a phospholipid dependent manner. New Phytologist 232: 2440-2456.

Saucedo-García, M., González-Solís, A., Rodríguez-Mejía, P., Lozano-Rosas, G., Olivera-Flores, T. de J., Carmona-Salazar, L., Guevara-García, A.A., Cahoon, E.B., Gavilanes-Ruíz, M., 2023. Sphingolipid long-chain base signaling in compatible and non-compatible plant pathogen interactions in *Arabidopsis*. International Journal of Molecular Sciences 24, 4384.

Saucedo-García, M., Guevara-García, A., González-Solís, A., Cruz-García, F., Vázquez-Santana, S., Markham, J.E., Lozano-Rosas, M.G., Dietrich, C.R., Ramos-Vega, M., Cahoon, E.B., Gavilanes-Ruíz, M., 2011. MPK6, sphinganine and the LCB2a gene from serine palmitoyltransferase are required in the signaling pathway that mediates cell death induced by long chain bases in *Arabidopsis*. New Phytologist 191, 943–957.

Schellenberger, R., Crouzet, J., Nickzad, A., Shu, L.-J., Kutschera, A., Gerster, T., Borie, N., Dawid, C., Cloutier, M., Villaume, S., Dhondt-Cordelier, S., Hubert, J., Cordelier, S., Mazeyrat-Gourbeyre, F., Schmid, C., Ongena, M., Renault, J.-H., Haudrechy, A., Hofmann, T., Baillieul, F., Clément, C., Zipfel, C., Gauthier, C., Déziel, E., Ranf, S., Dorey, S., 2021. Bacterial rhamnolipids and their 3-hydroxyalkanoate precursors activate *Arabidopsis* innate immunity through two independent mechanisms. Proceedings of the National Academy of Sciences U.S.A. 118, e2101366118.

1036 Schindelin, J., Arganda-Carreras, I., Frise, E., Kaynig, V., Longair, M., Pietzsch, T., Preibisch, S.,
1037 Rueden, C., Saalfeld, S., Schmid, B., Tinevez, J.-Y., White, D.J., Hartenstein, V., Eliceiri, K.,
1038 Tomancak, P., Cardona, A., 2012. Fiji: an open-source platform for biological-image analysis. Nature
1039 Methods 9, 676–682.
1040 Shi, L., Bielawski, J., Mu, J., Dong, H., Teng, C., Zhang, J., Yang, X., Tomishige, N., Hanada, K.,
1041 Hannun, Y.A., 2007. Involvement of sphingoid bases in mediating reactive oxygen intermediate
1042 production and programmed cell death in *Arabidopsis*. Cell Research 17, 1030.
1043 Ternes, P., Feussner, K., Werner, S., Lerche, J., Iven, T., Heilmann, I., Riezman, H., Feussner, I., 2011.
1044 Disruption of the ceramide synthase LOH1 causes spontaneous cell death in *Arabidopsis thaliana*.
1045 New Phytologist 192, 841–854.
1046 Torres, M.A., 2010. ROS in biotic interactions. Physiologia Plantarum 138, 414–429.
1047 Torres, M.A., Jones, J.D.G., Dangl, J.L., 2005. Pathogen-induced, NADPH oxidase–derived reactive
1048 oxygen intermediates suppress spread of cell death in *Arabidopsis thaliana*. Nature Genetics 37,
1049 1130–1134.
1050 Warren, R.F., Henk, A., Mowery, P., Holub, E., Innes, R.W., 1998. A mutation within the leucine-rich
1051 repeat domain of the *Arabidopsis* disease resistance gene RPS5 partially suppresses multiple
1052 bacterial and downy mildew resistance genes. The Plant Cell 10, 1439–1452.
1053 Wei, H.-L., Zhang, W., Collmer, A., 2018. Modular study of the type III effector repertoire in
1054 *Pseudomonas syringae* pv. *tomato* DC3000 reveals a matrix of effector interplay in pathogenesis. Cell
1055 Reports 23, 1630–1638.
1056 Whalen, M.C., Innes, R.W., Bent, A.F., Staskawicz, B.J., 1991. Identification of *Pseudomonas syringae*
1057 pathogens of *Arabidopsis* and a bacterial locus determining avirulence on both *Arabidopsis* and
1058 soybean. The Plant Cell 3, 49–59.
1059 Wirthmueller, L., Zhang, Y., Jones, J.D.G., Parker, J.E., 2007. Nuclear accumulation of the *Arabidopsis*
1060 immune receptor RPS4 is necessary for triggering EDS1-dependent defense. Current Biology 17,
1061 2023–2029.
1062 Xin, X.-F., Kvitko, B., He, S.Y., 2018. *Pseudomonas syringae*: what it takes to be a pathogen. Nature
1063 Reviews Microbiology 16, 316–328.
1064 Yoo, SD., Cho, YH., Sheen, J., 2007. *Arabidopsis* mesophyll protoplasts: a versatile cell system for
1065 transient gene expression analysis. Nature Protocols 2, 1565–1572.
1066 Yuan, M., Jiang, Z., Bi, G., Nomura, K., Liu, M., Wang, Y., Cai, B., Zhou, J.-M., He, S.Y., Xin, X.-F.,
1067 2021. Pattern-recognition receptors are required for NLR-mediated plant immunity. Nature 592, 105–
1068 109.
1069 Zheng, X., Spivey, N.W., Zeng, W., Liu, P.-P., Fu, Z.Q., Klessig, D.F., He, S.Y., Dong, X., 2012.
1070 Coronatine promotes *Pseudomonas syringae* virulence in plants by activating a signaling cascade that
1071 inhibits salicylic acid accumulation. Cell Host & Microbe 11, 587–596.
1072 Zhou, N., Tootle, T.L., Tsui, F., Klessig, D.F., Glazebrook, J., 1998. PAD4 functions upstream from
1073 salicylic acid to control defense responses in *Arabidopsis*. The Plant Cell 10, 1021–1030.
1074
1075

1076 **FIGURE LEGENDS**

1077 **Figure 1. Effect of co-infiltration of *Pst* and d18:0 on cell death.** (A) Representative
1078 leaves of Col-0 WT 48 hours after infiltration with either *Pst* DC3000, *Pst AvrRpm1*,
1079 *Pst AvrRpt2*, *Pst AvrRps4* alone or co-infiltrated with d18:0. The experiment was
1080 repeated at least 5 times with similar results (n=5). (B) Ion leakage measurements over
1081 24 hours following infiltration with *Pst AvrRpm1*, *Pst AvrRpt2* or *Pst AvrRps4*, alone or
1082 with d18:0. Data are reported as means ± SD (n=3). The experiment was repeated
1083 three times with similar results.

1084

1085 **Figure 2. *In vitro* and *in planta* bacterial growth in presence of sphinganine.** (A)
1086 Growth rate was estimated from bacterial growth curve data (OD_{600}) over 48 hours,
1087 ±SD in King's B medium. Asterisks indicate significant differences between each
1088 bacterium co-infiltrated with d18:0 or not (Wilcoxon-Mann-Whitney, *, $p<0.05$). (B)
1089 Bacterial growth ±SD (n = 3) at 0 and 48 hpi in *Arabidopsis* WT Col-0 leaves infected
1090 by bacteria alone or with d18:0.

1091

1092 **Figure 3. Extracellular ROS production in response to bacterial infection**.
1093 Extracellular ROS production measured in presence of *Pst AvrRpm1*, *Pst AvrRpt2 or*
1094 *Pst AvrRps4* with or without d18:0 in the medium. Data represent the sum of RLU
1095 (Relative Light Units) ± SEM (n = 6) over 90 min. The experiment was performed three
1096 times with similar results. Asterisks indicate significant differences between each
1097 bacterium co-infiltrated with d18:0 or not (Wilcoxon-Mann-Whitney; *, $p<0.05$).

1098

1099 **Figure 4. Late plant defense events in response to bacterial infiltration.** *Pst*
1100 DC3000 or *Pst AvrRpm1* were co-infiltrated with or without d18:0. (A) Camalexin was

1101 quantified at 0 and 48 hpi (FW: fresh weight). Different letters indicate significant
1102 differences (ANOVA, $p<0.05$, one way, n=5). (B) Representative leaves of *PR1::GUS*
1103 lines 48 hpi. (C) and (D) Relative expression of *PR1* and *VSP1*, respectively, followed
1104 6 and 48 hpi. Results are expressed as the fold increase in transcript level compared
1105 with the untreated control (0h), referred to as the x1 expression level. Experiments
1106 were repeated 3 times with similar results. (E) and (F) SA and JA-Isoleucine (JA-Ile)
1107 were quantified at 0 and 48 hpi. Different letters indicate significant differences
1108 (ANOVA, $p<0.05$, one way, n = 5).
1109
1110 **Figure 5. Involvement of RPM1 in the absence of defense responses**. (A)
1111 Photographs represent symptoms observed 72 hpi in WT, *rpm1-3*, *rpm1-rps2-rin4* and
1112 *RPM1-myc rpm1* lines treated with or without d18:0. (B) Western blot of RPM1 protein
1113 in WT and *RPM1-myc rpm1* line at 2, 6 or 24 hpi. Normalization was carried out with
1114 Actin. NT refers to non-treated samples. All experiments were repeated at least 3 times
1115 with similar results.
1116
1117 **Figure 6. Effect of *Pst AvrB* and *Pst AvrPphB* co-infiltration with d18:0 on plant**
1118 **defense responses.** (A) Photographs represent symptoms observed 48 hours after
1119 WT plant infiltration with either *Pst AvrB* or *Pst AvrPphB* alone or with d18:0. The
1120 experiment was repeated at least 3 times with similar results (n = 3). (B) Growth rate
1121 estimated from bacterial growth curve data (OD_{600}) over 48 hours, ±SD in King's B
1122 medium. (C) ROS production measurement in presence of *Pst AvrB* or *AvrPphB* with
1123 or without d18:0. Data represent the sum of RLU (Relative Light Units) ± SEM (n = 6)
1124 over 90 min. Experiments were performed three times with similar results. Asterisks
1125 indicate statistical differences (Wilcoxon-Mann-Whitney; *, $p<0.05$).

1126

1127 **Figure 7. *NMT1* expression in response to co-infiltration of bacteria and**
1128 **sphinganine.** Relative expression of *NMT1*, (N-*myristoyltransferase 1*) was followed
1129 at 6 and 48 hpi of *Pst* DC3000 or *Pst AvrRpm1* with or without d18:0. Results are
1130 expressed as the fold increase in transcript level compared with the untreated control
1131 (0h), referred to as the x1 expression level. Experiments were repeated three times
1132 with similar results. Asterisks indicate significant differences between each bacterium
1133 co-infiltrated with d18:0 or not (Wilcoxon-Mann-Whitney; *, $p<0.05$).

1134

1135 **Figure 8. Interaction of sphinganine with an implicit modeled bilayer.** (A) The
1136 Impala simulation calculates the energy restraints of a lipid bilayer as d18:0 goes
1137 through it. The X-axis corresponds to the position of the center of mass along the Z-
1138 axis. From left to right: the interface between the bilayer and the aqueous phase
1139 (orange), the interface between the polar head and the alkyl chain (pink) and the center
1140 of the bilayer (green). (B) The most energetically favorable orientation of d18:0 in the
1141 modeled bilayer. The lines represent the same planar surfaces as in A.

1142

1143 **Figure 9. Interaction of sphinganine with plant-like liposomes.** (A) Raw data from
1144 ITC experiments at 26°C. Each peak corresponds to a single injection of a 1 mM PLPC,
1145 glucosylceramide and sitosterol (60:20:20, molar ratio) LUV suspension into a solution
1146 containing 20 μM of d18:0. (B) Calculated thermodynamic parameters for this
1147 interaction. These values are means of two independent experiments. K represents
1148 the binding coefficient (the affinity of d18:0 for the LUVs), ΔG represents the molar free
1149 energy, ΔH, the molar enthalpy change, and TΔS, the molar entropy change.

1150

1151 **Figure 10. Specificity of sphinganine interaction with various lipids**
1152 **representative of the plant plasma membrane.** (A) Adsorption of d18:0 into
1153 monolayers of plant PM lipids: PLPC, glucosylceramide (GluCer) and β-sitosterol
1154 (Sito). d18:0 was injected at 1.25 µM in a subphase (Tris HCl, 10 mM, pH 7.4),
1155 underneath the lipid monolayer. The maximal insertion pressure (MIP) reflects the
1156 penetration power of d18:0 into the lipid monolayer and the differential Π (dΠ0)
1157 indicates the attracting effect the lipids have on it. (B) Total energies of interaction of
1158 d18:0 alone or with lipids representative of the plant plasma membrane were calculated
1159 with the Hypermatrix docking method. Lipids used were PLPC, GluCer, and Sito.
1160
1161 **Figure 11. Mechanical properties and organization of the plant plasma**
1162 **membrane in response to sphinganine treatment.** (A) to (C) Fluorescence
1163 red/green ratio images by multispectral confocal microscopy of a single-cell PM labeled
1164 with di-4-ANEPPDHQ after control (A), 2 µM d18:0 (B) or 5 µM d18:0 (C) treatment.
1165 (D) Red to green ratio of the PM (RGM) labeled with di-4-ANEPPDHQ treated with
1166 control (Ctrl), 2 µM or 5 µM d18:0. The asterisk indicates a significant difference
1167 compared to the control (P value < 0.05). (E) to (G) RGM profile on a 4 µm distance
1168 on PM from protoplasts after control (E), 2 µM d18:0 (F) or 5 µM d18:0 (G) treatment.
1169 (H) Variation of laurdan generalized polarization (ΔGP) measured in PM-mimicking
1170 liposomes (50 µM PLPC:Glucosylceramide: β-sitosterol (60:20:20 molar ratio)) at
1171 several time points after control (white bars) and 20 µM d18:0 treatment (grey bars). A
1172 positive ΔGP corresponds to a higher lipid packing within the bilayer. Mean ± SD of
1173 two replicates from four independent experiments. Asterisks indicate statistically
1174 significant differences with control, *P<0.05, **P<0.01, two-way ANOVA and Sidak's
1175 multiple comparison test. (I) Young's modulus measured on mesophyll protoplasts

1176 before or after 5 min incubation of d18:0 at two concentrations. Mean ± SD of at least
1177 50 analyses from three independent experiments. (J) Monolayer simulations of lipid-
1178 d18:0 interactions performed with Big Monolayer where each pixel represents a
1179 molecule. (Left) Plant lipid model with PLPC in green, glucosylceramide (GluCer) in
1180 blue and sitosterol (sito) in orange (60:20:20, molar ratio). (Right) The same lipids after
1181 addition of d18:0 in pink (88% lipids, 12% d18:0).
1182

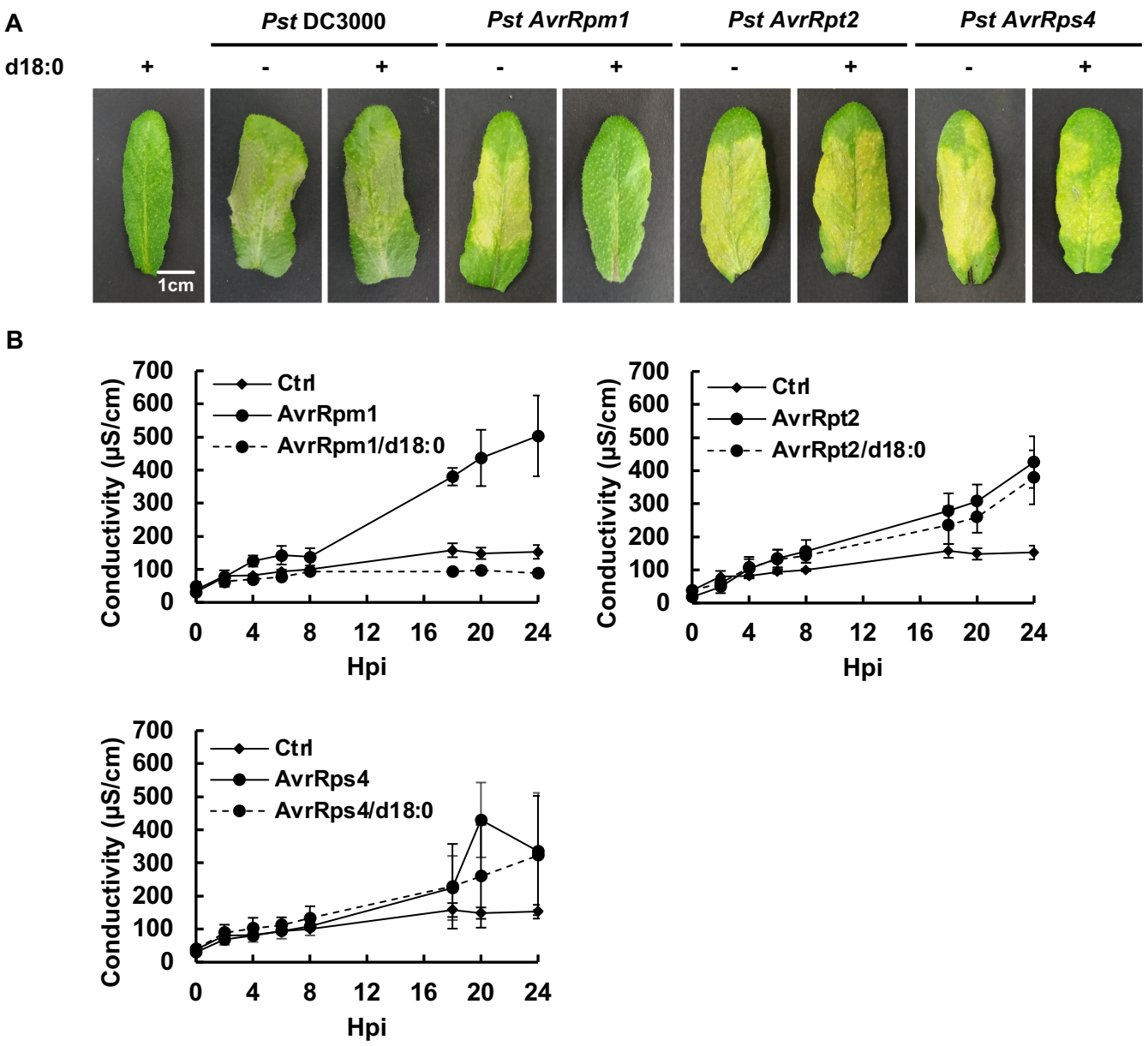

FIGURE 1 Effect of co-infiltration of *Pst* and d18:0 on cell death.
(A) Representative leaves of Col-0 WT 48 hours after infiltration with either *Pst* DC3000, *Pst AvrRpm1*, *Pst AvrRpt2*, *Pst AvrRps4* alone or co-infiltrated with d18:0. The experiment was repeated at least 5 times with similar results (n=5). (B) Ion leakage measurements over 24 hours following infiltration with *Pst AvrRpm1*, *Pst AvrRpt2* or *Pst AvrRps4*, alone or with d18:0. Data are reported as means ± SD (n=3). The experiment was repeated three times with similar results.

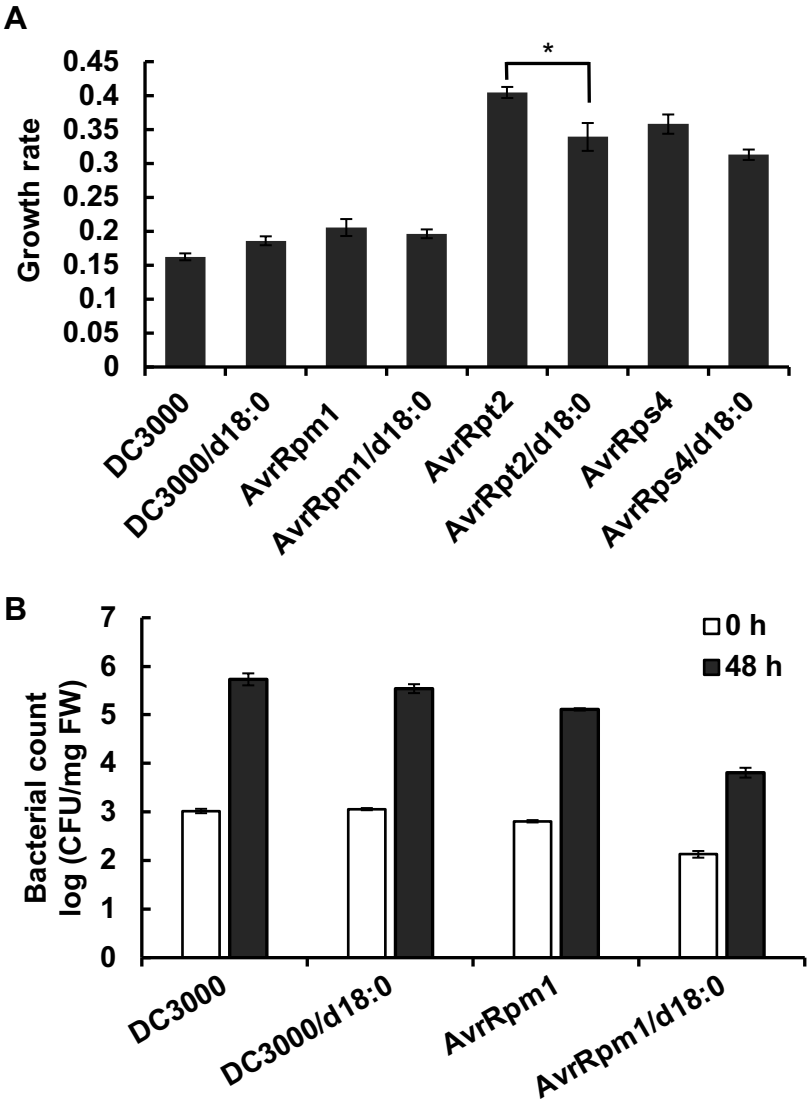

FIGURE 2 *In vitro* and *in planta* bacterial growth in presence of sphinganine. (A) Growth rate was estimated from bacterial growth curve data (OD_{600}) over 48 hours, ±SD in King's B medium. Asterisks indicate significant differences between each bacterium co-infiltrated with d18:0 or not (Wilcoxon-Mann-Whitney, *, $p<0.05$). (B) Bacterial growth ±SD (n = 3) at 0 and 48 hpi in *Arabidopsis* WT Col-0 leaves infected by bacteria alone or with d18:0.

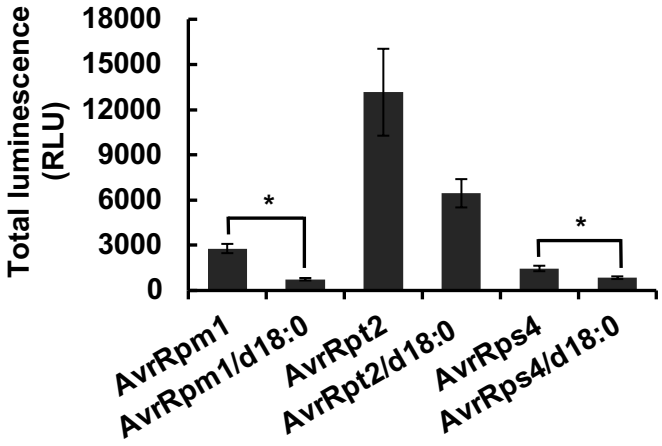

FIGURE 3 Extracellular ROS production in response to bacterial infection.
Extracellular ROS production measured in presence of *Pst AvrRpm1*, *Pst AvrRpt2 or Pst AvrRps4* with or without d18:0 in the medium. Data represent the sum of RLU (Relative Light Units) ± SEM (n = 6) over 90 min. The experiment was performed three times with similar results. Asterisks indicate significant differences between each bacterium co-infiltrated with d18:0 or not (Wilcoxon-Mann-Whitney; *, $p<0.05$).

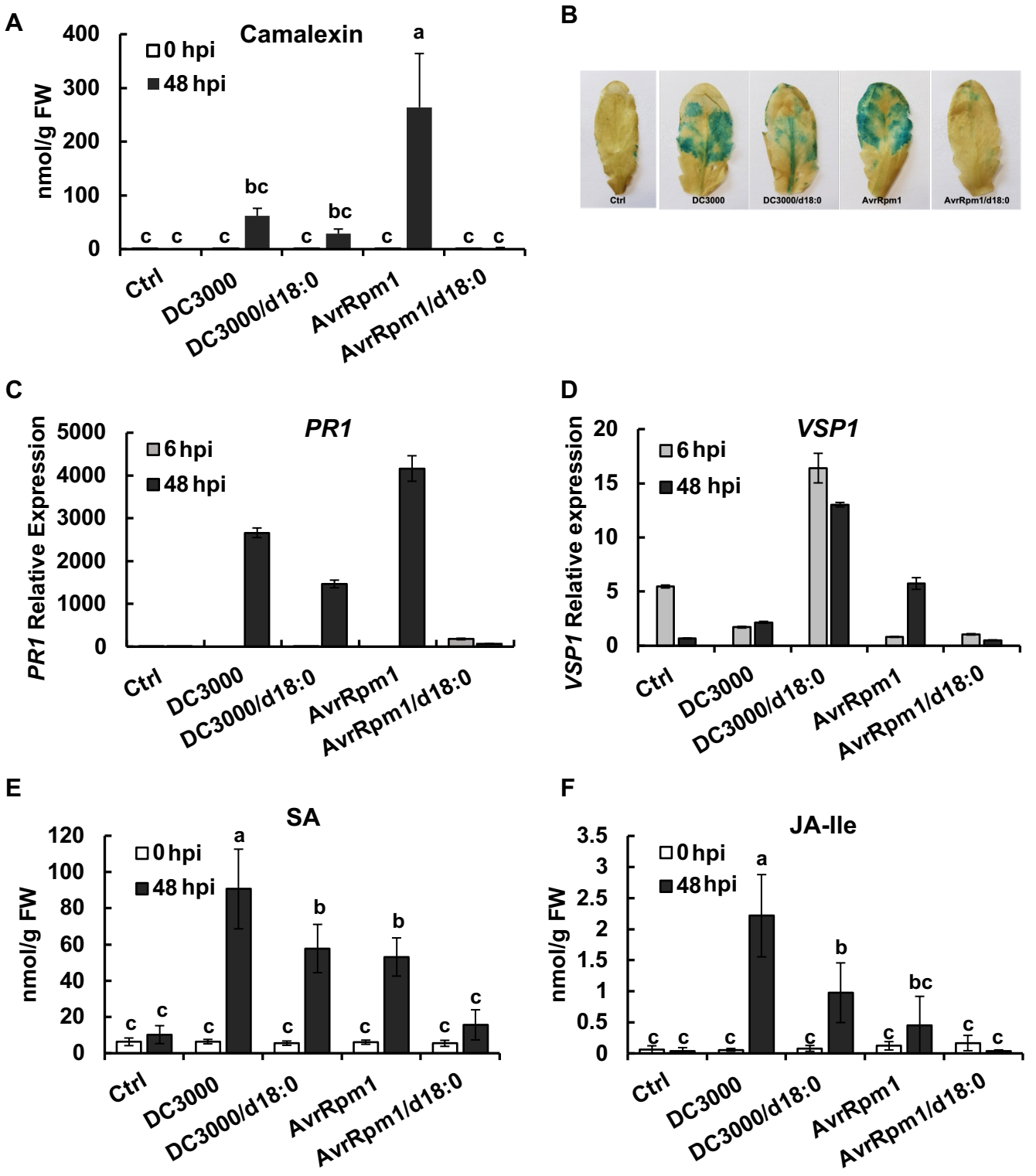

FIGURE 4 Late plant defense events in response to bacterial infiltration.
Pst DC3000 or *Pst AvrRpm1* were co-infiltrated with or without d18:0. (A) Camalexin was quantified at 0 and 48 hpi (FW: fresh weight). Different letters indicate significant differences (ANOVA, $p<0.05$, one way, n=5). (B) Representative leaves of *PR1::GUS* lines 48 hpi. (C) and (D) Relative expression of *PR1* and *VSP1*, respectively, followed 6 and 48 hpi. Results are expressed as the fold increase in transcript level compared with the untreated control (0h), referred to as the x1 expression level. Experiments were repeated 3 times with similar results. (E) and (F) SA and JA-Isoleucine (JA-Ile) were quantified at 0 and 48 hpi. Different letters indicate significant differences (ANOVA, $p<0.05$, one way, n = 5).

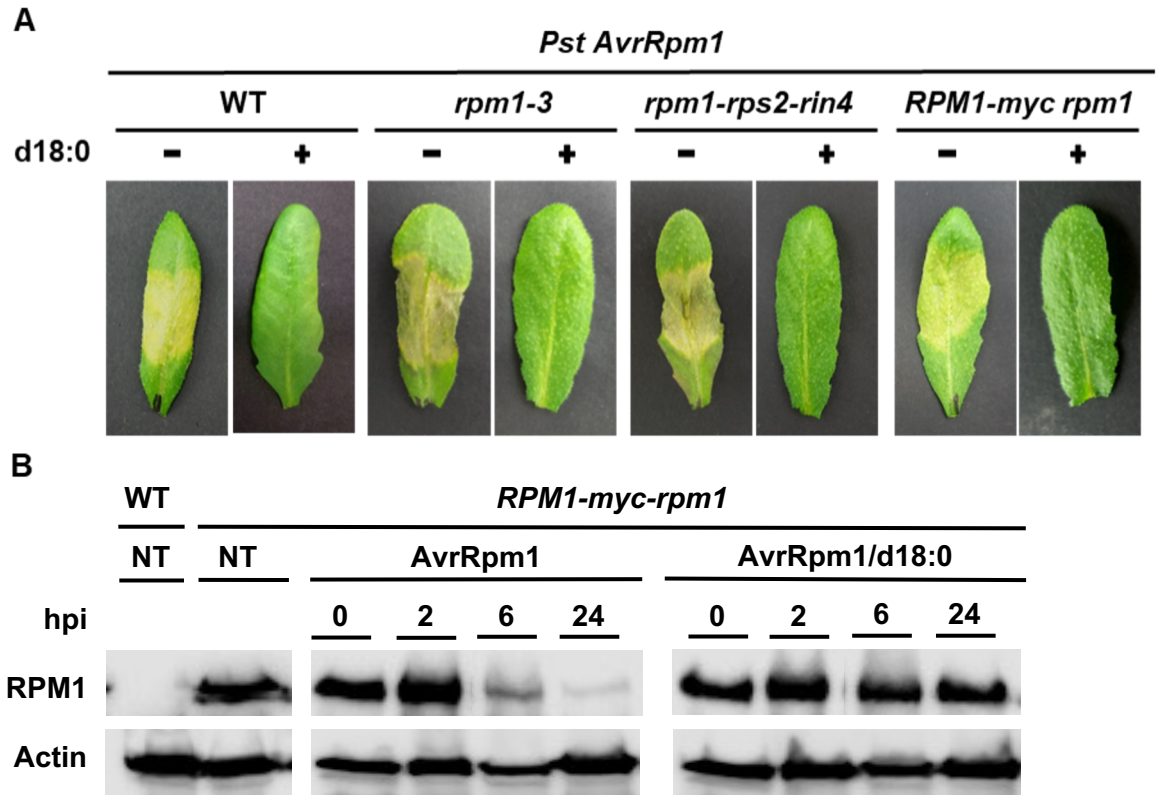

FIGURE 5 Involvement of RPM1 in the absence of defense responses.
(A) Photographs represent symptoms observed 72 hpi in WT, *rpm1-3*, *rpm1-rps2-rin4* and *RPM1-myc rpm1* lines treated with or without d18:0. (B) Western blot of RPM1 protein in WT and *RPM1-myc rpm1* line at 2, 6 or 24 hpi. Normalization was carried out with Actin. NT refers to non-treated samples. All experiments were repeated at least 3 times with similar results.

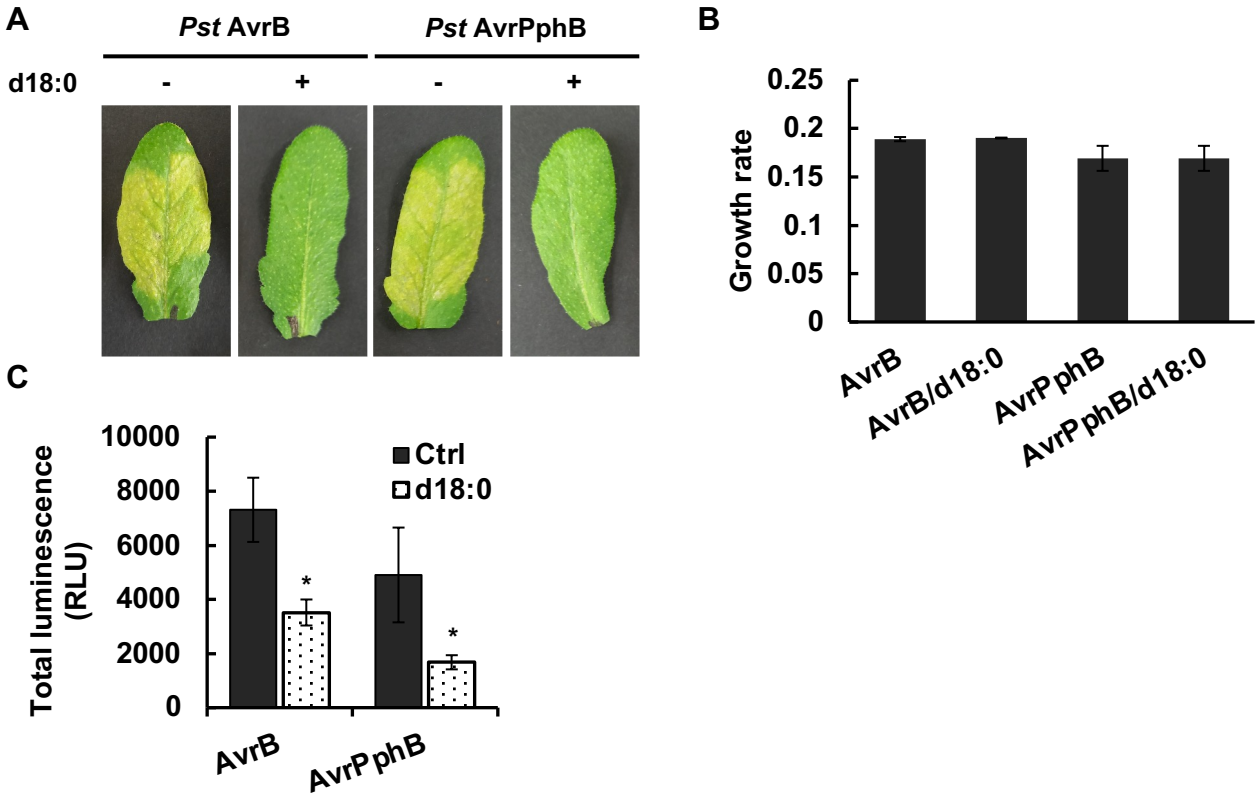

FIGURE 6 Effect of *Pst AvrB* and *Pst AvrPphB* co-infiltration with d18:0 on plant defense responses.

(A) Photographs represent symptoms observed 48 hours after WT plant infiltration with either *Pst AvrB* or *Pst AvrPphB* alone or with d18:0. The experiment was repeated at least 3 times with similar results (n = 3). (B) Growth rate estimated from bacterial growth curve data (OD_{600}) over 48 hours, ±SD in King's B medium. (C) ROS production measurement in presence of *Pst AvrB* or *AvrPphB* with or without d18:0. Data represent the sum of RLU (Relative Light Units) ± SEM (n = 6) over 90 min. Experiments were performed three times with similar results. Asterisks indicate statistical differences (Wilcoxon-Mann-Whitney; *, $p<0.05$).

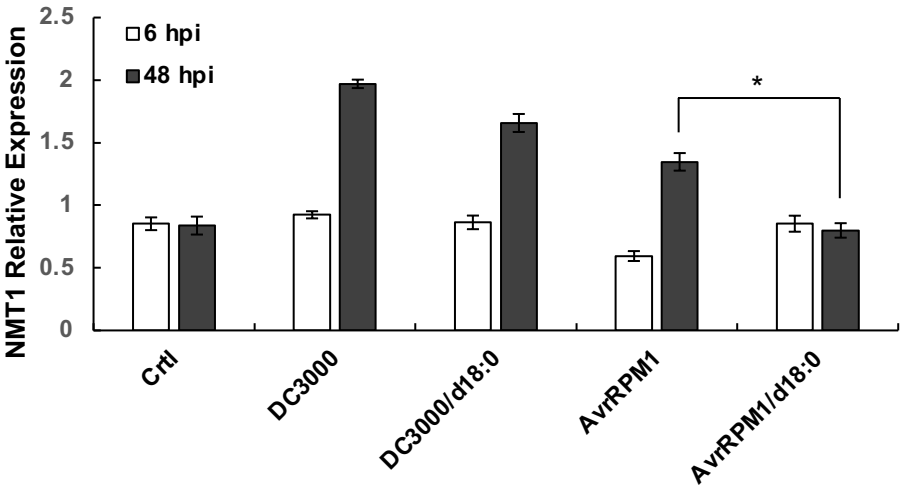

FIGURE 7 *NMT1* expression in response to co-infiltration of bacteria and sphinganine.

Relative expression of *NMT1*, (N-*myristoyltransferase 1*) was followed at 6 and 48 hpi of *Pst* DC3000 or *Pst AvrRpm1* with or without d18:0. Results are expressed as the fold increase in transcript level compared with the untreated control (0h), referred to as the x1 expression level. Experiments were repeated three times with similar results. Asterisks indicate significant differences between each bacterium co-infiltrated with d18:0 or not (Wilcoxon-Mann-Whitney; *, $p<0.05$).

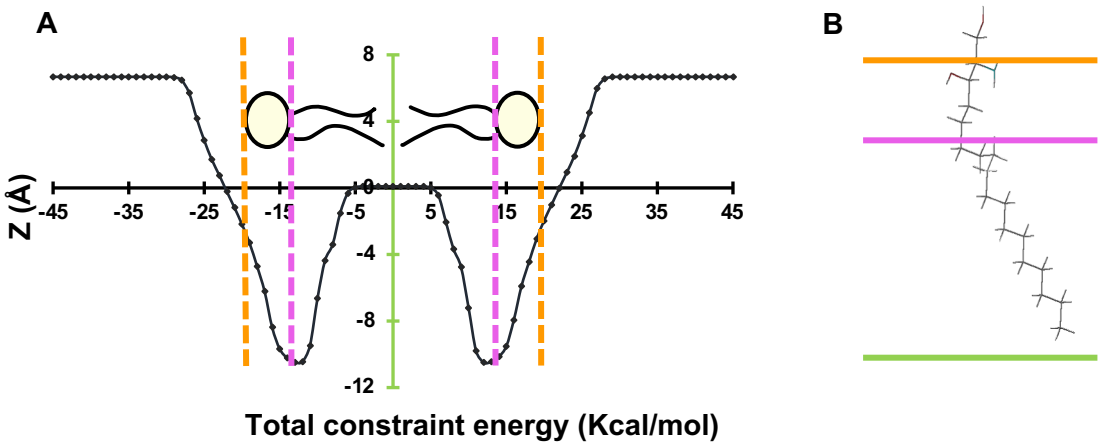

FIGURE 8 Interaction of sphinganine with an implicit modeled bilayer.
(A) The Impala simulation calculates the energy restraints of a lipid bilayer as d18:0 goes through it. The X-axis corresponds to the position of the center of mass along the Z-axis. From left to right: the interface between the bilayer and the aqueous phase (orange), the interface between the polar head and the alkyl chain (pink) and the center of the bilayer (green). (B) The most energetically favorable orientation of d18:0 in the modeled bilayer. The lines represent the same planar surfaces as in A.

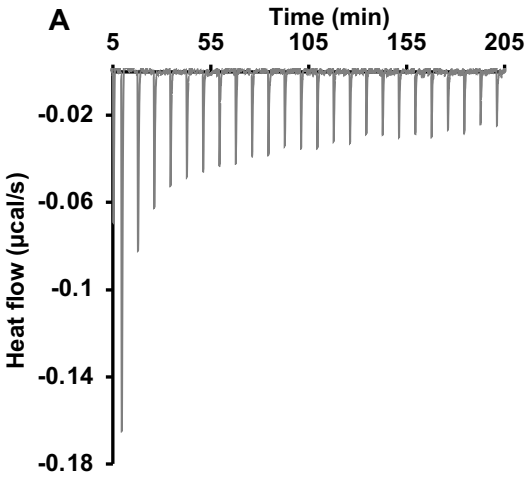

B

	Mean Values	Standard deviations
K (m/M)	86.80	18.99
ΔG (J/mol)	-16.09	0.55
ΔH (J/mol)	-1.39	0.26
TΔS (J/mol)	14.70	0.29

FIGURE 9 Interaction of sphinganine with plant-like liposomes. (A) Raw data from ITC experiments at 26°C. Each peak corresponds to a single injection of a 1 mM PLPC, glucosylceramide and sitosterol (60:20:20, molar ratio) LUV suspension into a solution containing 20 µM of d18:0. (B) Calculated thermodynamic parameters for this interaction. These values are means of two independent experiments. K represents the binding coefficient (the affinity of d18:0 for the LUVs), ΔG represents the molar free energy, ΔH, the molar enthalpy change, and TΔS, the molar entropy change.

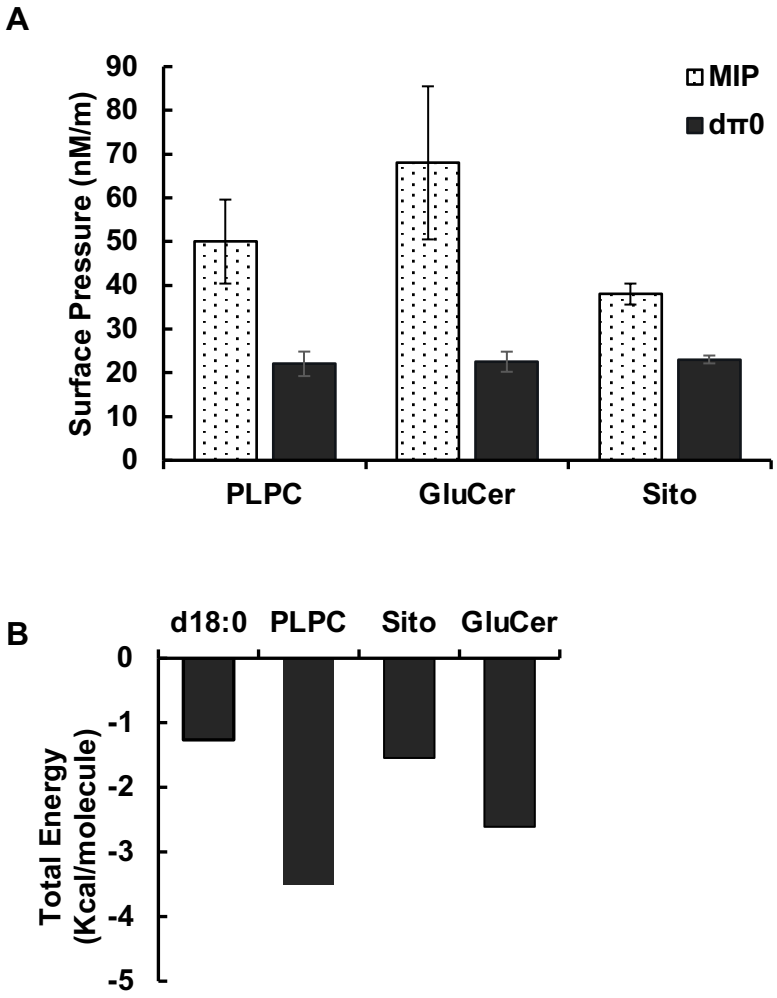

FIGURE 10 Specificity of sphinganine interaction with various lipids representative of the plant plasma membrane.
(A) Adsorption of d18:0 into monolayers of plant PM lipids: PLPC, glucosylceramide (GluCer) and b-sitosterol (Sito). d18:0 was injected at 1.25 μM in a subphase (Tris HCl, 10 mM, pH 7.4), underneath the lipid monolayer. The maximal insertion pressure (MIP) reflects the penetration power of d18:0 into the lipid monolayer and the differential Π (dΠ0) indicates the attracting effect the lipids have on it. (B) Total energies of interaction of d18:0 alone or with lipids representative of the plant plasma membrane were calculated with the Hypermatrix docking method. Lipids used were PLPC, GluCer, and Sito.

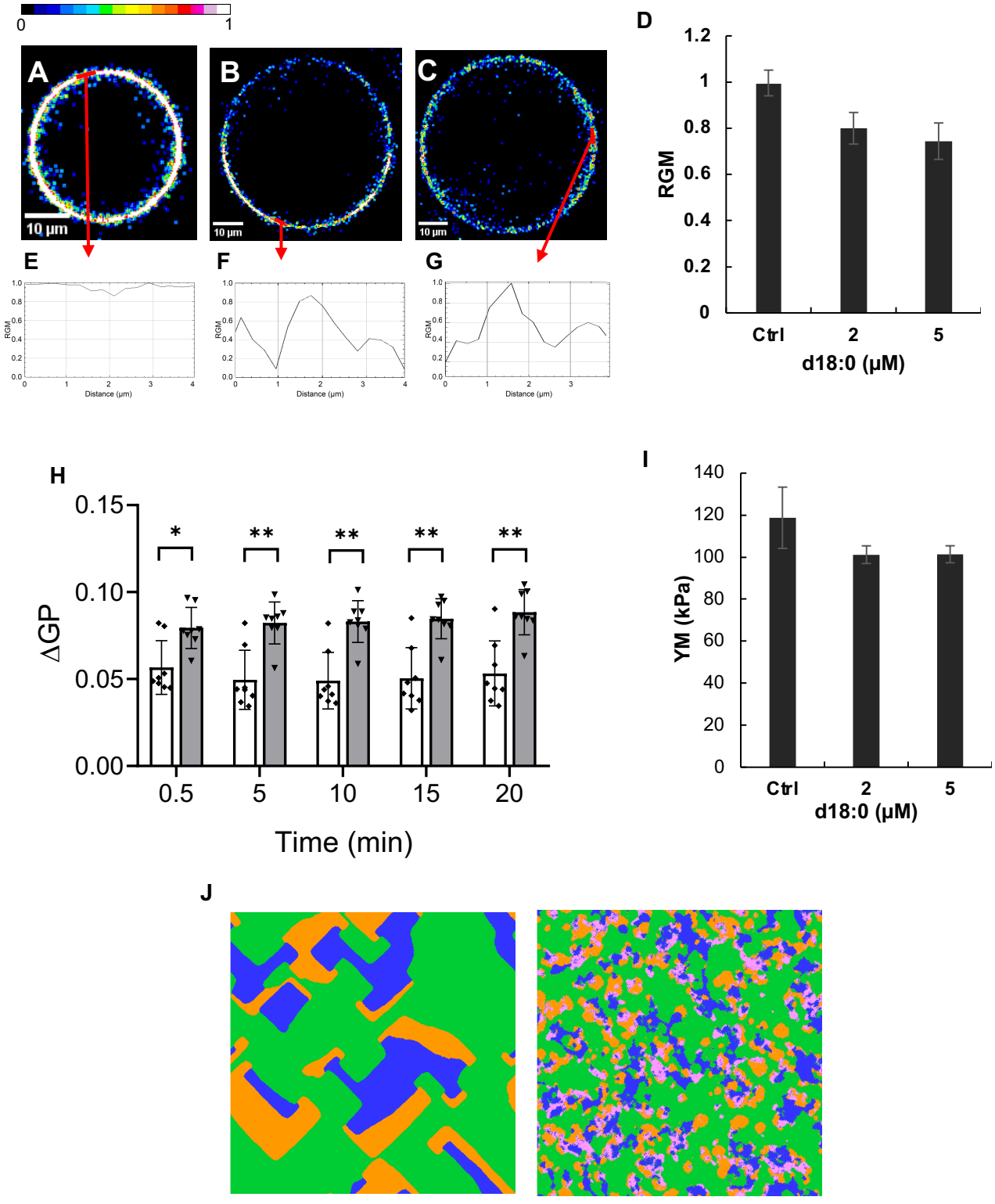

Figure 11. Mechanical properties and organization of the plant plasma membrane in response to sphinganine treatment.

(A) to (C) Fluorescence red/green ratio images by multispectral confocal microscopy of a single-cell PM labeled with di-4-ANEPPDHQ after control (A), 2 µM d18:0 (B) or 5 µM d18:0 (C) treatment. (D) Red to green ratio of the PM (RGM) labeled with di-4-ANEPPDHQ treated with control (Ctrl), 2 µM or 5 µM d18:0. The asterisk indicates a significant difference compared to the control (P value < 0.05). (E) to (G) RGM profile on a 4 µm distance on PM from protoplasts after control (E), 2 µM d18:0 (F) or 5 µM d18:0 (G) treatment. (H) Variation of laurdan generalized polarization (ΔGP) measured in PM-mimicking liposomes (50 µM PLPC:Glucosylceramide:β-sitosterol (60:20:20 molar ratio)) at several time points after control (white bars) and 20 µM d18:0 treatment (grey bars). A positive ΔGP corresponds to a higher lipid packing within the bilayer. Mean ± SD of two replicates from four independent experiments. Asterisks indicate statistically significant differences with control, *P<0.05, **P<0.01, two-way ANOVA and Sidak's multiple comparison test. (I) Young's modulus measured on mesophyll protoplasts before or after 5 min incubation of d18:0 at two concentrations. Mean ± SD of at least 50 analyses from three independent experiments. (J) Monolayer simulations of lipid-d18:0 interactions performed with Big Monolayer where each pixel represents a molecule. (Left) Plant lipid model with PLPC in green, glucosylceramide (GluCer) in blue and sitosterol (sito) in orange (60:20:20, molar ratio). (Right) The same lipids after addition of d18:0 in pink (88% lipids, 12% d18:0).